

Simplified two-layer models of precipitating atmosphere and their properties

J. Lambaerts,¹ G. Lapeyre,¹ V. Zeitlin,^{1,a)} and F. Bouchut²

¹Laboratoire de Météorologie Dynamique/IPSL, Ecole Normale Supérieure/CNRS/UPMC, 75005 Paris, France

²Laboratoire d'Analyse et de Mathématiques Appliquées, Université Paris-Est/CNRS, 77454 Marne-la-Vallée, France

(Received 4 January 2011; accepted 5 April 2011; published online 26 April 2011)

We derive a two-layer rotating shallow-water model for a moist atmosphere with water vapor condensation and related diabatic heating. Moist convection is represented by additional mass exchanges between the layers, which are determined from the moist enthalpy conservation principle, and related to the precipitation. Various boundary conditions at the lower and upper boundaries may be used. We show that the model reproduces in appropriate limits the main simplified models used previously in the literature for description of the large-scale moist-convective dynamics and precipitation fronts, namely the linear two-layer baroclinic models, the nonlinear two-layer quasigeostrophic model, and the nonlinear one-layer moist-convective rotating shallow-water model. We study the properties of the equations of the model, with special attention to the hyperbolicity loss, which is inherent to multilayer shallow-water models, and to the front propagation. Numerical illustrations of these properties are given with the help of a recently proposed high-resolution finite-volume numerical scheme with precipitation sources/sinks.

© 2011 American Institute of Physics. [doi:10.1063/1.3582356]

I. INTRODUCTION

In a preceding paper,¹ we derived a simple rotating shallow-water (RSW) type model for large-scale atmospheric dynamics that includes water vapor condensation and moist convection. We showed that the model was a natural nonlinear extension of the pioneering model by Gill,² which was extensively studied in the recent works of Majda and collaborators.^{3–5} In the model, the moist convection was represented by a mass sink related to a convective flux through the upper boundary of the fluid layer. This flux, in turn, was proportional to precipitation, which was triggered once a saturation threshold in the humidity was attained. In spite of its nice properties,¹ the model remains essentially barotropic and should be thought of as a part of a fully baroclinic system, where the mass loss would become a mass exchange between the layers. In the present paper, we derive such a fully baroclinic two-layer moist-convective RSW (mc2RSW) model. We show that the one-layer model is a limit of the infinitely thick upper layer of the parent model. We also show how the balanced moist-convective two-layer model of Ref. 6 follows from our model in the quasigeostrophic limit. These limits prove that our two-layer model is sound. We also examine in detail the mathematical and physical properties of the new model, as well as its variants resulting from different choices of boundary conditions.

The paper is organized as follows. In Sec. II, we present a derivation of the model by vertical averaging of the primitive equations, and by use of the moist enthalpy conservation. In Sec. III, we study the physical and mathematical

properties of the model, and in particular of its one-dimensional (1D) version. The behavior of the characteristics is studied and we address the question of (possible) loss of hyperbolicity. The Rankine–Hugoniot conditions are derived for weak solutions, and the properties of the precipitation fronts are analyzed. In Sec. IV, we study a reduction of the model resulting from imposing the constant pressure (“rigid bottom,” instead of free material surface) boundary condition; this allows us to filter out the global modes and to restrict attention to the most important baroclinic modes. In Sec. V, we establish the one-layer and quasigeostrophic limits of our model and show how one recovers the models known in the literature. In Sec. VI, we present examples of numerical simulations with the model, illustrating its basic properties in the simplest nonrotating one-dimensional configuration. Section VII contains conclusions and a discussion. A variant of the model with the mass flux through the upper boundary, which should be rather considered as the lower part of a more complicated three-(or more) layer system, is briefly discussed in Appendix A. Appendix B contains a generalization to nonconstant relaxation threshold for precipitation.

II. DERIVATION OF THE TWO-LAYER RSW EQUATIONS WITH MOIST CONVECTION

We start from the primitive equations in pseudoheight isobaric coordinates⁷

$$\frac{d}{dt}\mathbf{v} + f\mathbf{k} \times \mathbf{v} = -\nabla\phi, \quad (2.1)$$

^{a)}Author to whom correspondence should be addressed. Electronic mail: zeitlin@lmd.ens.fr.

$$\frac{d}{dt}\theta=0, \quad (2.2)$$

$$\nabla \cdot \mathbf{v} + \partial_z w = 0, \quad (2.3)$$

$$\partial_z \phi = g \frac{\theta}{\theta_0}. \quad (2.4)$$

Here, $\mathbf{v}=(u,v)$ denotes the horizontal velocity field, $(d/dt) = \partial_t + \mathbf{v} \cdot \nabla + w \partial_z$ denotes the Lagrangian derivative, $\nabla = (\partial_x, \partial_y)$, w is the vertical velocity, and f is the Coriolis parameter, which will be considered constant for simplicity in what follows. \mathbf{k} is the unit vector in the z -direction, g is gravitational acceleration, θ is potential temperature, θ_0 is a normalization constant (potential temperature on the ground), and ϕ is geopotential. It should be remembered⁷ that an approximation of constant in the vertical (in pseudoheight coordinate \bar{z}) pseudodensity r , defined as $r d\bar{z} = \rho dz$, where ρ is the air density and z is geometric height, is made in the model in order to arrive at the incompressibility condition [Eq. (2.3)].

The system [Eqs. (2.1)–(2.4)] describes the dry adiabatic dynamics of the atmosphere, where evaporation of water and condensation of the water vapor are switched off. The specific humidity q is conserved during the motion of air parcels

$$\frac{d}{dt}q=0. \quad (2.5)$$

In the presence of precipitation (the evaporation will be not considered throughout the paper, although it may be easily added), the potential temperature (=entropy) Eq. (2.2) and the specific humidity Eq. (2.5) acquire a source and a sink, respectively. Nevertheless, there still exists a Lagrangian invariant, the moist enthalpy (ME) $\theta + (L/c_p)q$, where L is the latent heat release coefficient and c_p is the specific heat.⁸ On the isobaric surface, this quantity is conserved for any air parcel

$$\frac{d}{dt}\left(\theta + \frac{L}{c_p}q\right) = 0. \quad (2.6)$$

Our goal is to obtain vertically averaged primitive equations for large-scale atmospheric motions, including the precipitation effects. As is well known,⁹ vertical averaging of the “dry” Eqs. (2.1)–(2.4) between consecutive material surfaces leads to multilayer RSW equations. One could try to average the full “moist” version of these equations. This would lead, however, to substantial difficulties due to the essential nonlinearity of the equation of state of the moist air and of the resulting expressions for source and sinks, to be added to Eqs. (2.2) and (2.5), respectively. We would rather adopt another, heuristic, approach. Precipitation leads to latent heat release and related moist convection. We will try to incorporate these phenomena in the traditional shallow-water setting by adding appropriate sinks/sources, like we have already done while deriving the simplest one-layer moist-

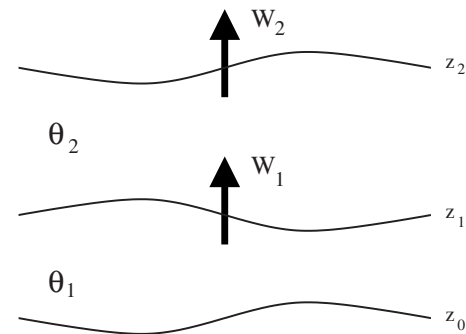


FIG. 1. Sketch of the atmospheric two-layer RSW model with mass exchanges through the boundaries via additional vertical velocities W_1 and W_2 .

convective RSW model.¹ For simplicity, we will limit ourselves to two-layer configurations, multilayer generalizations being straightforward.

We thus consider three material surfaces $z_k(x,y,t)$ ($k=0,1,2$) with moist-convective fluxes represented by additional vertical velocities W_1 and W_2 through the upper boundaries, as shown in Fig. 1,

$$\begin{cases} w_0 = \frac{dz_0}{dt}, \\ w_1 = \frac{dz_1}{dt} + W_1, \\ w_2 = \frac{dz_2}{dt} + W_2. \end{cases} \quad (2.7)$$

Under the hypothesis of constant pseudodensity, the extra vertical velocity indeed corresponds to a mass flux. The explicit form of these fluxes will be obtained below from the moist enthalpy conservation.

The hydrostatic relation Eq. (2.4) is integrated in z in each layer, giving the following expressions for the geopotential:

$$\phi(z) = \begin{cases} \phi(z_0) + g \frac{\theta_1}{\theta_0}(z - z_0), & \text{if } z_0 \leq z \leq z_1, \\ \phi(z_0) + g \frac{\theta_1}{\theta_0}(z_1 - z_0) + g \frac{\theta_2}{\theta_0}(z - z_1), & \text{if } z_1 \leq z \leq z_2, \end{cases} \quad (2.8)$$

where $\theta_{1,2}$ are averaged potential temperatures in the lower and upper layers $\{z_0, z_1\}$ and $\{z_1, z_2\}$, respectively. We vertically average the equations of the system [Eqs. (2.1)–(2.3)] in each layer using Eqs. (2.7) and (2.8), and the mean field approximation: $\langle ab \rangle \approx \langle a \rangle \langle b \rangle$. Furthermore, we suppose that the averaged potential temperature remains horizontally homogeneous in each layer (otherwise so-called Ripa’s equations result, instead of the standard RSW¹): $\nabla \theta_i = 0$. We thus obtain the momentum

$$\left\{ \begin{array}{l} \partial_t \mathbf{v}_1 + (\mathbf{v}_1 \cdot \nabla) \mathbf{v}_1 + f \mathbf{k} \times \mathbf{v}_1 = -\nabla \phi(z_1) + g \frac{\theta_1}{\theta_0} \nabla z_1, \\ \partial_t \mathbf{v}_2 + (\mathbf{v}_2 \cdot \nabla) \mathbf{v}_2 + f \mathbf{k} \times \mathbf{v}_2 = -\nabla \phi(z_2) + g \frac{\theta_2}{\theta_0} \nabla z_2 \\ \quad + \frac{\mathbf{v}_1 - \mathbf{v}_2}{h_2} W_1, \end{array} \right. \quad (2.9)$$

and the mass conservation equations

$$\left\{ \begin{array}{l} \partial_t h_1 + \nabla \cdot (h_1 \mathbf{v}_1) = -W_1, \\ \partial_t h_2 + \nabla \cdot (h_2 \mathbf{v}_2) = +W_1 - W_2, \end{array} \right. \quad (2.10)$$

in both layers, where $\mathbf{v}_i = \langle \mathbf{v} \rangle_i$, $\langle \cdot \rangle_i$ means the vertical average over the layer i , and $h_i = z_i - z_{i-1}$ is the thickness of the layer i . h_i is directly proportional to the mass of the layer since pseudodensity is supposed to be constant. Equations (2.9) and (2.10) are the equations of the two-layer RSW model with (yet undetermined) mass exchanges and no boundary conditions imposed at z_0 and z_2 . Such general configuration is presented in Fig. 1. It should be mentioned that the last term of the second equation in Eq. (2.9) represents a vertical transfer of momentum by convection and follows in the approximation $\mathbf{v}(z_i) \approx \mathbf{v}_i$. Note that such term also appears in the three-layer model developed similar to our considerations in Ref. 10.

We now vertically integrate the ME conservation Eq. (2.6) and obtain the following:

$$\left\{ \begin{array}{l} \Delta_1 \left[\theta_1 h_1 + \frac{L}{c_p} Q_1 \right] = - \left\{ \theta(z_1) + \frac{L}{c_p} q(z_1) \right\} W_1, \\ \Delta_2 \left[\theta_2 h_2 + \frac{L}{c_p} Q_2 \right] = + \left\{ \theta(z_1) + \frac{L}{c_p} q(z_1) \right\} W_1 \\ \quad - \left\{ \theta(z_2) + \frac{L}{c_p} q(z_2) \right\} W_2, \end{array} \right. \quad (2.11)$$

where $Q_i = \int_{z_{i-1}}^{z_i} q dz$ is the bulk humidity in the corresponding layer, and we defined $\Delta_i[a] = \partial_t a + \nabla \cdot (a \mathbf{v}_i)$. Using the constancy of potential temperature and the mass conservation Eq. (2.10), these expressions are rewritten as follows:

$$\left\{ \begin{array}{l} \frac{L}{c_p} \Delta_1[Q_1] = - \left\{ \theta(z_1) + \frac{L}{c_p} q(z_1) - \theta_1 \right\} W_1, \\ \frac{L}{c_p} \Delta_2[Q_2] = + \left\{ \theta(z_1) + \frac{L}{c_p} q(z_1) - \theta_2 \right\} W_1 \\ \quad - \left\{ \theta(z_2) + \frac{L}{c_p} q(z_2) - \theta_2 \right\} W_2. \end{array} \right. \quad (2.12)$$

Then we can explicitly link W_i to the precipitation P_i in the corresponding layer by supposing that precipitation is the only moisture sink

$$\partial_t Q_i + \nabla \cdot (Q_i \mathbf{v}_i) = -P_i. \quad (2.13)$$

In the precipitating regions ($P_i > 0$), moisture is saturated $q(z_i) = q^s(z_i)$ and the temperature of the air mass $dx dy W_i dt$ convected due to the latent heat release $\theta(z_i) + (L/c_p) q^s(z_i)$ must correspond to the temperature of the upper layer θ_{i+1} .

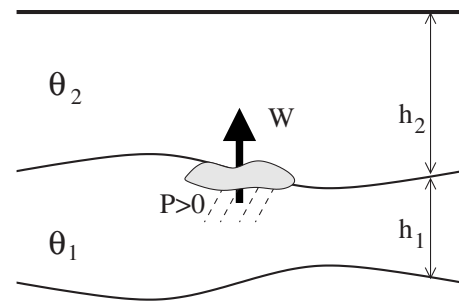


FIG. 2. Sketch of the mc2RSW model.

By choosing a “dry” stable stratification of the atmosphere,

$$\theta_{i+1} = \theta(z_i) + \frac{L}{c_p} q(z_i) \approx \theta_i + \frac{L}{c_p} q(z_i) > \theta_i, \quad (2.14)$$

with constant $\theta(z_i)$ and $q(z_i)$, we get from Eqs. (2.12) and (2.13) that mass sinks are proportional to precipitation,

$$W_i = \beta_i P_i, \quad (2.15)$$

with a positive-definite coefficient

$$\beta_i = \frac{L}{c_p (\theta_{i+1} - \theta_i)} \approx \frac{1}{q(z_i)} > 0. \quad (2.16)$$

Here, θ_3 is an undefined potential temperature above z_2 .

The last step of the derivation consists of linking the precipitation to the bulk humidity. To do this, we will use a Betts–Miller-type scheme. The original one¹¹ corresponds to the relaxation by precipitation of the specific humidity q to a vertical convective reference profile $q^c(z)$. We apply a vertically averaged version of the relaxation by assuming that the bulk humidity in each layer Q_i relaxes to a reference value associated to the saturation value Q_i^s . For simplicity, the latter is chosen constant, but it can also depend on the layer thickness h_i (see Appendix B)

$$P_i = \frac{Q_i - Q_i^s}{\tau} H(Q_i - Q_i^s) \quad (2.17)$$

where $H(\cdot)$ is the Heaviside function.

Equations (2.9), (2.10), (2.13), (2.15), and (2.17) are to be completed by boundary conditions. More precisely, one has to make assumptions on the character of the surfaces $z_k(x, y, t)$ and on their geopotentials $\phi(z_k)$. In the following Secs. III and IV and in Appendix A, we derive three variants of the moist-convective two-layer RSW model (mc2RSW) and analyze their properties.

III. THE TWO-LAYER MOIST-CONVECTIVE RSW MODEL (MC2RSW)

A. The model

In the first variant of the two-layer model, which is sketched in Fig. 2, the upper boundary is “rigid” (isobaric), $z_2 = \text{const}$, while the geopotential of the bottom boundary remains constant, $\phi(z_0) = \text{const}$, as in the standard representation of the ground if the pressure is used as the vertical coordinate.¹² Since moisture is usually concentrated in the

lower atmosphere, we suppose that $Q_2=0$ and that convective flux through the top boundary is zero, $W_2=0$.

In this case, Eqs. (2.9), (2.10), and (2.13) become

$$\partial_t \mathbf{v}_1 + (\mathbf{v}_1 \cdot \nabla) \mathbf{v}_1 + f \mathbf{k} \times \mathbf{v}_1 = -g \nabla (h_1 + h_2), \quad (3.1)$$

$$\partial_t \mathbf{v}_2 + (\mathbf{v}_2 \cdot \nabla) \mathbf{v}_2 + f \mathbf{k} \times \mathbf{v}_2 = -g \nabla (h_1 + \alpha h_2) + \frac{\mathbf{v}_1 - \mathbf{v}_2}{h_2} \beta P, \quad (3.2)$$

$$\partial_t h_1 + \nabla \cdot (h_1 \mathbf{v}_1) = -\beta P, \quad (3.3)$$

$$\partial_t h_2 + \nabla \cdot (h_2 \mathbf{v}_2) = +\beta P, \quad (3.4)$$

$$\partial_t Q + \nabla \cdot (Q \mathbf{v}_1) = -P, \quad (3.5)$$

where $\alpha = \theta_2 / \theta_1$ is the stratification parameter and for simplicity we take $\theta_0 = \theta_1$ and omit the index 1: $W_1 = W$, $P_1 = P$, $\beta_1 = \beta$, and $Q_1 = Q$. The precipitation term is given by Eq. (2.17) with a constant saturation value $Q_1^s = Q^s$.

B. Conservation laws

Dropping a constant pseudodensity factor, the energy density of each layer is defined as

$$\begin{cases} e_1 = h_1 \frac{\mathbf{v}_1^2}{2} + g \frac{h_1^2}{2}, \\ e_2 = h_2 \frac{\mathbf{v}_2^2}{2} + gh_1 h_2 + \alpha g \frac{h_2^2}{2}, \end{cases} \quad (3.6)$$

and one can show that for the total energy of the isolated system $E = \int dx (e_1 + e_2)$, we get the following:

$$\partial_t E = - \int dx \beta P \left(gh_2 (1 - \alpha) + \frac{(\mathbf{v}_1 - \mathbf{v}_2)^2}{2} \right). \quad (3.7)$$

The first term in the right-hand side (rhs) is positive for a stable stratification $\alpha > 1$ and corresponds to the production of potential energy while the second term is always negative and corresponds to the destruction of kinetic energy due to the drag produced by convective mass exchange. At the zeroth order in perturbations over the state of rest, precipitation thus increases the energy, which is consistent with our intuition on latent heat release

$$\partial_t E \approx - \int dx \beta P g H_2 (1 - \alpha). \quad (3.8)$$

As follows from Eq. (3.6), we work with the *dry* energy, which will be just called energy hereafter. An example of ‘‘moist’’ energy functional may be found in Refs. 3 and 6.

As follows from Eqs. (3.3) and (3.4), the mass of each layer is not conserved, but the total mass of the system is constant.

Moist enthalpy in the lower layer is defined by $m_1 = h_1 - \beta Q$ and is always locally conserved

$$\partial_t m_1 + \nabla \cdot (m_1 \mathbf{v}_1) = 0. \quad (3.9)$$

Since the upper layer is dry ($Q_2=0$), the moist enthalpy is not defined there.

Momentum equations in each layer are derived by combining Eqs. (3.1), (3.3), (3.2), and (3.4), pairwise

$$\begin{aligned} (\partial_t + \mathbf{v}_1 \cdot \nabla) (\mathbf{v}_1 h_1) + \mathbf{v}_1 h_1 \nabla \cdot \mathbf{v}_1 + f \mathbf{k} \times (\mathbf{v}_1 h_1) \\ = -g \nabla \frac{h_1^2}{2} - gh_1 \nabla h_2 - \mathbf{v}_1 \beta P, \end{aligned} \quad (3.10)$$

$$\begin{aligned} (\partial_t + \mathbf{v}_2 \cdot \nabla) (\mathbf{v}_2 h_2) + \mathbf{v}_2 h_2 \nabla \cdot \mathbf{v}_2 + f \mathbf{k} \times (\mathbf{v}_2 h_2) \\ = -\alpha g \nabla \frac{h_2^2}{2} - gh_2 \nabla h_1 + \mathbf{v}_1 \beta P. \end{aligned} \quad (3.11)$$

The second term in the rhs of each equation takes into account the mutual influence of the layers and does not allow us to rewrite these equations in a conservative form, even in the absence of the Coriolis force. The last term in each equation represents a drag due to moist convection, which also appears in the three-layer model of Ref. 10. It acts as an effective friction and diminishes the energy, cf. Eq. (3.7). The sum of Eqs. (3.10) and (3.11) in the absence of rotation ($f=0$) gives local conservation of the total momentum $\mathbf{v}_1 h_1 + \mathbf{v}_2 h_2$. This latter is thus not affected by the moist processes.

Potential vorticity (PV) plays an important role in rotating fluids. Its evolution in each layer is given by

$$(\partial_t + \mathbf{v}_1 \cdot \nabla) \frac{\zeta_1 + f}{h_1} = \frac{\zeta_1 + f}{h_1^2} \beta P, \quad (3.12)$$

$$\begin{aligned} (\partial_t + \mathbf{v}_2 \cdot \nabla) \frac{\zeta_2 + f}{h_2} = - \frac{\zeta_2 + f}{h_2^2} \beta P \\ + \frac{\mathbf{k}}{h_2} \cdot \left\{ \nabla \times \left(\frac{\mathbf{v}_1 - \mathbf{v}_2}{h_2} \beta P \right) \right\}, \end{aligned} \quad (3.13)$$

where $\zeta_i = \mathbf{k} \cdot (\nabla \times \mathbf{v}_i) = \partial_x v_i - \partial_y u_i$ ($i=1, 2$) is the relative vorticity. Thus, PV in each layer is not a Lagrangian invariant in the precipitating regions. The main source term, $(-1)^{i-1} (\zeta_i + f) h_i^{-2} \beta P$, reinforces (weakens) PV in the lower (upper) layer. This is in agreement with the previous results in the one-layer mcRSW model.¹³ Another source appears in the upper layer PV Eq. (3.13) and represents the vorticity induced by the drag due to moist convection.

Conservation of the moist enthalpy in the lower layer Eq. (3.9) allows us to derive a new Lagrangian invariant, the moist potential vorticity (MPV)

$$(\partial_t + \mathbf{v}_1 \cdot \nabla) \frac{\zeta_1 + f}{m_1} = 0. \quad (3.14)$$

There is no equivalent of this quantity in the upper layer.

C. Mathematical properties

1. Characteristic equation

As usual, in studying the hyperbolic structure of the mc2RSW equations (which may be anticipated from what is known of its ‘‘dry’’ counterpart), reducing the spatial dimensions allows us to make explicit calculations. The 1.5-dimensional (1.5D) version of the system [Eqs. (3.1)–(3.5)]

(i.e., with all dependence on one spatial coordinate, y , removed, but velocity in y -direction remaining) can be rewritten in the standard quasilinear form

$$\partial_t \mathbf{f} + \mathbf{A}(\mathbf{f}) \partial_y \mathbf{f} = \mathbf{b}(\mathbf{f}). \tag{3.15}$$

where \mathbf{f} is a vector representing the variables $(u_1, v_1, u_2, v_2, h_1, h_2, Q)$, \mathbf{A} is a matrix given by

$$\mathbf{A} = \begin{pmatrix} u_1 & 0 & 0 & 0 & g & g & 0 \\ 0 & u_1 & 0 & 0 & 0 & 0 & 0 \\ 0 & 0 & u_2 & 0 & g & \alpha g & 0 \\ 0 & 0 & 0 & u_2 & 0 & 0 & 0 \\ h_1 & 0 & 0 & 0 & u_1 & 0 & 0 \\ 0 & 0 & h_2 & 0 & 0 & u_2 & 0 \\ Q & 0 & 0 & 0 & 0 & 0 & u_1 \end{pmatrix}, \tag{3.16}$$

and \mathbf{b} is the vector of the source/sink terms given by

$$\mathbf{b} = \begin{pmatrix} +fv_1 \\ -fu_1 \\ +fv_2 + \frac{u_1 - u_2}{h_2} \beta P \\ -fu_2 + \frac{v_1 - v_2}{h_2} \beta P \\ -\beta P \\ +\beta P \\ -P \end{pmatrix}. \tag{3.17}$$

A quasilinear system is hyperbolic only when the eigenvalues of the matrix \mathbf{A} are real.¹⁴ In this case, they correspond to propagation velocities along the characteristics $c(x, t)$. Solving the eigenproblem $\det(\mathbf{A} - c\mathbf{I}) = 0$, where \mathbf{I} is the unit matrix, leads to the following characteristic equation:

$$\mathcal{F}(c) = \{(u_1 - c)^2 - gh_1\} \{(u_2 - c)^2 - \alpha gh_2\} - gh_1 gh_2 = 0, \tag{3.18}$$

if nonpropagating characteristics ($c = u_1$ and $c = u_2$) are discarded. This is a fourth-order algebraic equation that may not have real solutions.

The linearization of Eq. (3.18) around a state of rest allows us to obtain an approximation of the characteristics for small perturbations. The solutions are as follows:

$$C_{\pm} = g(H_1 + \alpha H_2) \frac{1 \pm \sqrt{\Delta}}{2}, \tag{3.19}$$

where we use the notation $C = c^2$ and

$$\Delta = 1 - \frac{4H_1 H_2 (\alpha - 1)}{(H_1 + \alpha H_2)^2} = \frac{(H_1 - \alpha H_2)^2 + 4H_1 H_2}{(H_1 + \alpha H_2)^2}. \tag{3.20}$$

These solutions may be related to the speeds of dry linear gravity waves in the system. For a stable stratification ($\alpha > 1$), it is easy to show that $0 < \Delta < 1$ and $C_{\pm} > 0$, which means that the four linear characteristic velocities c are real and that the system Eq. (3.15) linearized (in its hydrodynamical part) around the state of rest is hyperbolic. The slow

solutions C_- correspond to *internal* characteristics due to their strong baroclinic components. By analogy, the fast, mostly barotropic, solutions C_+ may be called *external*.¹⁵

When precipitation is taken into account, we will analyze the system under the assumption of immediate relaxation: $\tau \rightarrow 0$. This is a reasonable simplification, as the time-scale of the relaxation toward saturated humidity in the atmosphere is rather small (between 2 and 12 h). This limit corresponds to the strict quasiequilibrium hypothesis and is singular in the sense that the system becomes *piecewise hyperbolic*. In the nonprecipitating areas ($P = 0$), the same results as above are valid, while in the precipitating areas the precipitation term can be rewritten in terms of wind convergence in the lower layer,² $P = -Q^s \nabla \cdot \mathbf{v}_1$, which modifies the properties of the system (such approximation was systematically derived in the one-layer case¹). Consequently, the system [Eqs. (3.1)–(3.5)] takes the following form:

$$\partial_t \mathbf{v}_1 + (\mathbf{v}_1 \cdot \nabla) \mathbf{v}_1 + f \mathbf{k} \times \mathbf{v}_1 = -g \nabla (h_1 + h_2), \tag{3.21}$$

$$\begin{aligned} \partial_t \mathbf{v}_2 + (\mathbf{v}_2 \cdot \nabla) \mathbf{v}_2 + f \mathbf{k} \times \mathbf{v}_2 = & -g \nabla (h_1 + \alpha h_2) \\ & - \frac{\mathbf{v}_1 - \mathbf{v}_2}{h_2} \beta Q^s \nabla \cdot \mathbf{v}_1, \end{aligned} \tag{3.22}$$

$$\partial_t h_1 + \nabla \cdot (h_1 \mathbf{v}_1) = +\beta Q^s \nabla \cdot \mathbf{v}_1, \tag{3.23}$$

$$\partial_t h_2 + \nabla \cdot (h_2 \mathbf{v}_2) = -\beta Q^s \nabla \cdot \mathbf{v}_1, \tag{3.24}$$

while the humidity field is always staying at its saturation value: $Q = Q^s$.

The characteristic equation for the 1.5D version of the system [Eqs. (3.21)–(3.24)] is given by

$$\mathcal{F}^m(c) = \mathcal{F}(c) + \mathcal{R} g \beta Q^s = 0, \tag{3.25}$$

where

$$\mathcal{R} = (u_1 - u_2)^2 - (\alpha - 1) gh_2. \tag{3.26}$$

Linearizing Eq. (3.25) leads to the following moist linear characteristic velocities:

$$C_{\pm}^m = g(H_1 + \alpha H_2) \frac{1 \pm \sqrt{\Delta^m}}{2}. \tag{3.27}$$

The discriminant is modified by precipitation with respect to the dry one [Eq. (3.20)],

$$\Delta^m = 1 - \frac{4M_1 H_2 (\alpha - 1)}{(H_1 + \alpha H_2)^2} = \Delta + \frac{4(\alpha - 1) \beta Q^s H_2}{(H_1 + \alpha H_2)^2}. \tag{3.28}$$

For a stable stratification ($\alpha > 1$), it is easy to show that $C_{\pm}^m > 0$, and hence corresponding c^m are real, for a positive moist enthalpy of the lower layer in the state of rest: $M_1 = H_1 - \beta Q^s > 0$. The linearized system [Eqs. (3.21)–(3.24)] is then hyperbolic under this assumption.

Comparison of the dry and the moist linear characteristic velocities gives

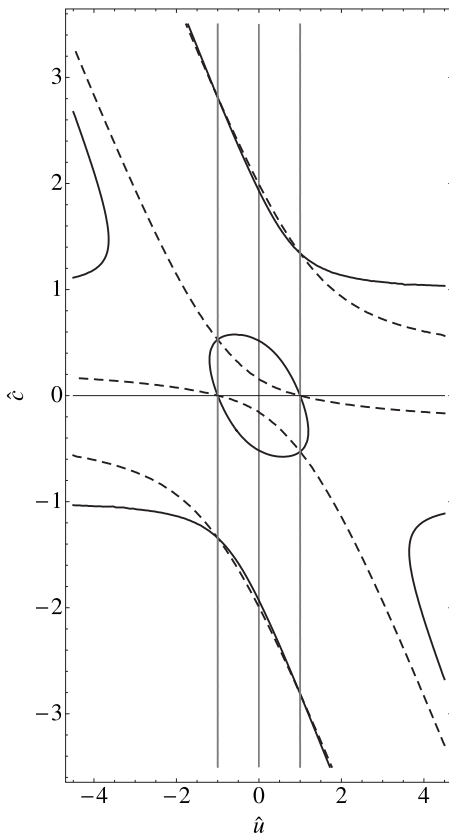


FIG. 3. Normalized solutions $\hat{c}=(c-u_1)/\sqrt{gh_1}$ of the dry and moist characteristic equations $\mathcal{F}(c)=0$ [Eq. (3.18)] (solid) and $\mathcal{F}^m(c)=0$ [Eq. (3.25)] (dashed), respectively, as functions of the normalized baroclinic velocity $\hat{u}=(u^{bc})/\sqrt{gh_1}$. Vertical gray lines correspond to solutions of $\mathcal{R}=0$ for which the dry and moist characteristic velocities are identical: $|\hat{u}|=1$. Here, $\gamma=h_1/h_2=0.5$, $\alpha=1.5$, and $\beta Q^s/h_1=0.9$.

$$C_-^m < C_- < \frac{g(H_1 + \alpha H_2)}{2} < C_+ < C_+^m, \tag{3.29}$$

for $0 < M_1 < H_1$. Thus, in the model, the moist internal (mainly baroclinic) mode propagates more slowly than the dry one, which is consistent with the observations.¹⁶

These results can be compared with numerical solutions of nonlinear characteristic Eqs. (3.18) and (3.25) for a given set of parameters. Figure 3 shows the dry (solid) and the moist (dashed) characteristic velocities as functions of the baroclinic velocity $u^{bc}=u_1-u_2$. Two of the four dry solutions (corresponding to the internal characteristic velocities) become complex for $1.2 \leq |u^{bc}|/\sqrt{gh_1} \leq 3.6$ while all of the moist ones stay real. The result [Eq. (3.29)] is well verified for $u^{bc}=0$ and one observes that it is maintained in the nonlinear case until $|u^{bc}|/\sqrt{gh_1}=1$ for the chosen values of parameters. This limit corresponds to $\mathcal{R}=0$, denoted by solid gray lines in the figure.

2. Criterion of hyperbolicity

The hyperbolicity of the system is preserved if all four solutions c of the characteristic Eq. (3.18) are real. In the previous section, we showed that this is guaranteed around the state of rest. Now we attempt to define a criterion of

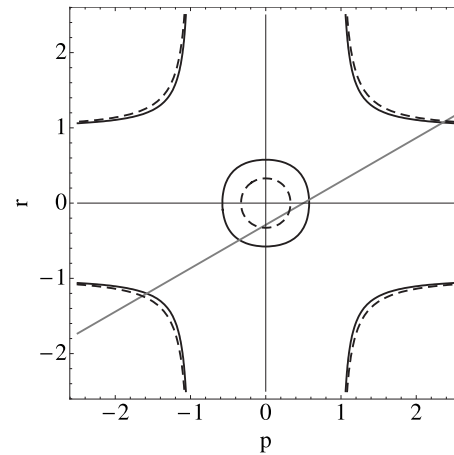


FIG. 4. The curves [Eq. (3.30)] (solid) and [Eq. (3.36)] (dashed) and the straight line [Eq. (3.32)] in the (p, r) -plane. $\gamma=h_1/h_2=0.5$, $\alpha=1.5$, $\beta Q^s/h_1=0.9$, and $u^{bc}/\sqrt{gh_1}=0.5 < 1$.

hyperbolicity (still in the 1.5D system) globally, by using the method proposed by Ovsyannikov.¹⁷ The characteristic Eq. (3.18) can be written in the form

$$(p^2 - 1)(r^2 - 1) = \frac{1}{\alpha}, \tag{3.30}$$

with

$$p = \frac{u_1 - c}{\sqrt{gh_1}} \quad \text{and} \quad r = \frac{u_2 - c}{\sqrt{\alpha gh_2}}. \tag{3.31}$$

The solutions can be found as intersections of the curve defined by Eq. (3.30) and the straight line

$$r = \sqrt{\frac{h_1}{\alpha h_2}} p - \frac{u^{bc}}{\sqrt{\alpha gh_2}}, \tag{3.32}$$

in the (p, r) plane, as follows from Eq. (3.31). For $p^2 > 1$ and $r^2 > 1$, the solutions of Eq. (3.30) are simply

$$r = \pm \sqrt{1 + \frac{1}{\alpha(p^2 - 1)}} \tag{3.33}$$

and possess straight asymptotes at $p = \pm 1$ and $r = \pm 1$. For $p^2 < 1$ and $r^2 < 1$, Eq. (3.30) is close to the one of the circle $p^2 + r^2 = \text{constant}$, and solutions can be expressed as functions of the polar angle Θ

$$p = \sqrt{\frac{\alpha - 1}{\alpha}} \cos \Theta \quad \text{and} \quad r = \sqrt{\frac{\alpha - 1}{\alpha \sin^2 \Theta + \cos^2 \Theta}} \sin \Theta. \tag{3.34}$$

These solutions are shown in Fig. 4.

By a simple geometric argument, it is possible to obtain a sufficient condition for the existence of four intersection points between these two curves in the (p, r) plane: the straight line must cross the circle of radius $\sqrt{(\alpha - 1)/\alpha}$. This imposes the following condition on the vertical shear:

$$\frac{|u^{bc}|}{\sqrt{gh_1}} \leq \begin{cases} \sqrt{\frac{\alpha-1}{\gamma}} & \text{if } \gamma \leq \alpha, \\ \sqrt{\frac{\alpha-1}{\alpha}} & \text{if } \gamma \geq \alpha, \end{cases} \quad (3.35)$$

where $\gamma = h_1/h_2$. Note that this condition corresponds to $\mathcal{R} = 0$ for $\gamma \leq \alpha$.

In the precipitating regions in the immediate relaxation approximation, the characteristic Eq. (3.25) becomes

$$(p^2 - 1)(r^2 - 1) = \frac{1}{\alpha} - \frac{\mathcal{R}\beta Q^s}{\alpha gh_1 h_2}. \quad (3.36)$$

Solutions similar to the previous one can be derived if $\mathcal{R} < gh_1 h_2 / \beta Q^s$, which is an additional constraint on the vertical shear

$$\frac{|u^{bc}|}{\sqrt{gh_1}} < \sqrt{\frac{\alpha-1 + \frac{h_1}{\beta Q^s}}{\gamma}}, \quad (3.37)$$

where $h_1 / \beta Q^s > 1$ for positive moist enthalpy. In this case, the sufficient condition for the existence of four intersections between the two curves consists of a straight line crossing the circle of radius $\sqrt{(\alpha-1)/\alpha + \mathcal{R}\beta Q^s / \alpha gh_1 h_2}$, and thus

$$\frac{|u^{bc}|}{\sqrt{gh_1}} \leq \begin{cases} \sqrt{\frac{\alpha-1}{\gamma}} & \text{if } \gamma \leq \alpha, \\ \sqrt{\frac{\alpha-1}{\gamma} \frac{h_1 - \beta Q^s}{ah_2 - \beta Q^s}} & \text{if } \gamma \geq \alpha. \end{cases} \quad (3.38)$$

Note that in the particular case $ah_2 - \beta Q^s \leq 0$, the existence of the four intersections is directly satisfied and no other condition for the vertical shear than Eq. (3.37) is needed.

In conclusion, for positive moist enthalpy $m_1 = h_1 - \beta Q^s$, the hyperbolicity criterion is the same (if $\gamma \leq \alpha$), or looser (if $\gamma \geq \alpha$), in the moist as compared to the dry case.

It is important to stress that the conditions Eqs. (3.35) and (3.38) together with Eq. (3.37) are sufficient but not necessary. Furthermore, even if Eq. (3.37) is not satisfied, the system may be hyperbolic in precipitating regions where $P_{\tau=0} > 0$ while not hyperbolic in nonprecipitating regions.

In Fig. 3, the hyperbolicity limits [Eqs. (3.35) and (3.38)] are the same and are indicated by the gray lines corresponding to $\mathcal{R} = 0$ since $\gamma < \alpha$. One observes that the hyperbolicity in nonprecipitating regions is lost for the internal characteristic velocities, which become complex, while the hyperbolicity in the precipitating regions is preserved beyond this limit. Note that this happens for $\mathcal{R} > 0$ when the inequality between dry and moist characteristic velocities is not satisfied anymore, see Eq. (3.29).

3. Linearized Riemann variables

A quasilinear system [Eq. (3.15)] can be rewritten in the characteristic form¹⁴

$$I_j(\partial_t + c_j \partial_x) \mathbf{f} = I_j \mathbf{b}(\mathbf{f}) \quad (3.39)$$

where c_j is the eigenvalue of the $n \times n$ matrix \mathbf{A} and I_j —the associated left eigenvector ($j = 1, \dots, n$). For some systems,

this form can be simplified by a change of variables to give

$$(\partial_t + c_j \partial_x) r_j = g_j. \quad (3.40)$$

In this case, it describes the evolution of solutions r_j , called Riemann variables, along the characteristic curves c_j . If $g_j = 0$, the Riemann variables become Riemann invariants.

The form of solutions c_k ($k = 1, \dots, 4$) of Eq. (3.18) is too complicated to formulate the 1.5D system [Eqs. (3.1)–(3.5)] in the form of Eq. (3.39) or Eq. (3.40). Nonetheless, a linearized solution is always possible, especially in the absence of rotation, and is useful in order to show how precipitation affects the dry solutions.

By linearizing the hydrodynamic part of the one-dimensional version of Eqs. (3.1)–(3.5) in the absence of rotation around the state of rest (H_1, H_2, \bar{Q}) and by neglecting the second-order precipitation term in the momentum equation, the system is reduced to

$$\begin{cases} (\partial_t + c_k \partial_x) r_k = \left(-\frac{c_k}{H_1} + \left(\frac{c_k^2}{gH_1} - 1 \right) \frac{c_k}{H_2} \right) \beta P, \\ \partial_t r_0 = - \left(1 - \frac{\beta \bar{Q}}{H_1} \right) P, \end{cases} \quad (3.41)$$

where the characteristic velocities c_k are the positive and negative square roots of Eq. (3.19) and the Riemann variables are given by

$$\begin{cases} r_k = u_1 + \frac{c_k}{H_1} \eta_1 + \left(\frac{c_k^2}{gH_1} - 1 \right) \left(u_2 + \frac{c_k}{H_2} \eta_2 \right), \\ r_0 = q - \frac{\bar{Q}}{H_1} \eta_1, \end{cases} \quad (3.42)$$

where $h_i = H_i + \eta_i$ ($i = 1, 2$) and $Q = \bar{Q} + q$. Precipitation modifies the Riemann variable on each characteristic curve. This modification strongly depends on the value of c_k . In the immediate relaxation limit ($\tau \rightarrow 0$), the system is piecewise hyperbolic and the characteristic form of the 1D linearized version of Eqs. (3.21)–(3.24) in the precipitating region is given by

$$(\partial_t + c_k^m \partial_x) r_k^m = 0, \quad (3.43)$$

where the moist Riemann variables

$$\begin{aligned} r_k^m = u_1 + & \left(\frac{c_k^m}{M_1} - \frac{\left(\frac{c_k^{m2}}{gM_1} - 1 \right) \beta Q^s c_k^m}{1 + \frac{\beta Q^s c_k^{m2}}{M_1 gH_2}} \right) \eta_1 \\ & + \frac{\frac{c_k^{m2}}{gM_1} - 1}{1 + \frac{\beta Q^s c_k^{m2}}{M_1 gH_2}} \left(u_2 + \frac{c_k^m}{H_2} \eta_2 \right) \end{aligned} \quad (3.44)$$

are invariant ($M_1 = H_1 - \beta Q^s$). This result is in agreement with the nonlinear results obtained previously in the one-layer model.¹

4. Fronts and Rankine–Hugoniot conditions

In this subsection, we will study the propagation of discontinuities, both in dynamical variables and their derivatives, which will be frequently called fronts below. We will be particularly interested in precipitation fronts: the boundaries between precipitating and nonprecipitating regions. Discontinuities correspond to weak solutions of a hyperbolic system and their propagation must satisfy the Rankine–Hugoniot (RH) conditions deduced from the conservation equations for mass and momentum.¹⁴

a. Shocks: Discontinuities in dynamical variables. A complete system of the RH conditions describing the jumps of the dynamical variables across discontinuities (shocks), and thus completely determining the weak solutions, may be obtained for a system of conservation laws.¹⁸ The exchange terms $gh_1\nabla h_2$ and $gh_2\nabla h_1$ appearing in the momentum Eqs. (3.10) and (3.11) prevent us from rewriting these equations in the conservative form $\partial_t f_j + \nabla \cdot \mathbf{F}_j(\mathbf{f}) = d_j(\mathbf{f})$. Only the mass in each layer and the total momentum ($\mathbf{v}_1 h_1 + \mathbf{v}_2 h_2$) are locally conserved. The available RH conditions for the 1.5D system [Eqs. (3.1)–(3.5)] may be derived by standard rules

$$\left\{ \begin{array}{l} -s[u_1 h_1 + u_2 h_2] \\ \quad + \left[u_1^2 h_1 + u_2^2 h_2 + g \frac{h_1^2}{2} + g \alpha \frac{h_2^2}{2} + gh_1 h_2 \right] = 0, \\ -s[v_1 h_1] + [u_1 v_1 h_1] = 0, \\ -s[v_2 h_2] + [u_2 v_2 h_2] = 0, \\ -s[h_1] + [h_1 u_1] = 0, \\ -s[h_2] + [h_2 u_2] = 0, \\ -s[Q] + [Q u_1] = 0, \end{array} \right. \quad (3.45)$$

where here and below s is the velocity of propagation of the discontinuity and $[\dots]$ is a jump across this discontinuity. We emphasize here that, as in the mcRSW model,¹ precipitation does not appear in these relations because in the integrated equations, $\lim_{x_s \rightarrow a} \lim_{b \rightarrow x_s} \int_a^b P = 0$, where x_s is the position of the discontinuity. Since P is a continuous function of Q , it simply inherits its jump. Even if $[P]$ exists, it only appears in the RH conditions for the derivatives of the dynamical variables and does not directly affect the shock propagation.

As the conditions [Eq. (3.45)] are not complete, with one more condition missing, an additional constraint must be chosen to close the system. This point has been largely discussed in the literature, in particular, in the context of gravity currents. Reduced models under additional hypotheses of weak stratification or thin upper layer have been derived in order to simplify the RH conditions, so that additional constraint is no more needed.¹⁹ Since shocks dissipate energy, the additional constraint was usually chosen to represent the energy loss in one of the layers depending on the type of shock.^{20,21} Holland *et al.*²² introduced a turbulent internal energy in the energy equation to take into account the dissipation by mixing. Jiang and Smith²³ developed an ideal shock theory by parametrizing the small scale turbulence by Newtonian or non-Newtonian viscosity term in the momen-

tum equation. The closure problem of the RH conditions in a two-layer SW model still remains open. We will come back to this discussion in Sec. VI.

In the particular case of a discontinuity inside a precipitating region in the immediate relaxation limit ($\tau \rightarrow 0$), the jump in humidity $[Q]$ is impossible since $Q = Q^s$, and all the conditions [Eq. (3.45)] except for the first are modified correspondingly,

$$\left\{ \begin{array}{l} -s[v_1 h_1 + v_2 h_2] + [u_1 v_1 h_1 + u_2 v_2 h_2] = 0, \\ -s[m_1] + [m_1 u_1] = 0, \\ -s[h_2] + [h_2 u_2 + \beta Q^s u_1] = 0. \end{array} \right. \quad (3.46)$$

The condition derived from the mass conservation in the lower layer h_1 is replaced by the one derived from the moist enthalpy conservation $m_1 = h_1 - \beta Q^s$. Two additional constraints are now needed to close the system.

b. Discontinuities in the derivatives of dynamical variables and precipitation fronts. In the immediate relaxation limit $\tau \rightarrow 0$, precipitation can be considered to be discontinuous at the interface between precipitating and nonprecipitating regions. The jump $[P]$ appears only in the RH conditions for the derivatives of the dynamical variables, and corresponds to a weak discontinuity. The associated RH conditions are derived from the integration of the conservation laws for the derivatives of the dynamical variables. Contrary to the momentum equations (3.10) and (3.11), the equations for the *derivatives* of the momentum in each layer do have a conservative form,

$$\left\{ \begin{array}{l} \partial_{tx}(u_1 h_1) + \partial_{xx} \left(u_1^2 h_1 + g \frac{h_1^2}{2} \right) \\ \quad + \partial_x(gh_1 \partial_x h_2) - f \partial_x(v_1 h_1) = -\beta \partial_x(u_1 P), \\ \partial_{tx}(u_2 h_2) + \partial_{xx} \left(u_2^2 h_2 + \alpha g \frac{h_2^2}{2} \right) \\ \quad + \partial_x(gh_2 \partial_x h_1) - f \partial_x(v_2 h_2) = +\beta \partial_x(u_1 P), \\ \partial_{tx}(v_1 h_1) + f \partial_x(u_1 h_1) = -\beta \partial_x(v_1 P), \\ \partial_{tx}(v_2 h_2) + f \partial_x(u_2 h_2) = +\beta \partial_x(v_1 P), \end{array} \right. \quad (3.47)$$

so a full system of RH conditions is as follows:

$$\left\{ \begin{array}{l} (u_1 - s)[\partial_x u_1] + g[\partial_x h_1] + g[\partial_x h_2] = 0, \\ (u_2 - s)[\partial_x u_2] + g[\partial_x h_1] + \alpha g[\partial_x h_2] = \frac{u_1 - u_2}{h_2} [P], \\ (u_1 - s)[\partial_x v_1] = 0, \\ (u_2 - s)[\partial_x v_2] = \frac{v_1 - v_2}{h_2} [P], \\ (u_1 - s)[\partial_x h_1] + h_1[\partial_x u_1] = -\beta [P], \\ (u_2 - s)[\partial_x h_2] + h_2[\partial_x u_2] = +\beta [P], \\ (u_1 - s)[\partial_x Q] + Q^s[\partial_x u_1] = -[P], \end{array} \right. \quad (3.48)$$

where dynamical variables themselves are supposed to be continuous. Discarding the nonpropagating solutions $s = u_1$ and $s = u_2$, these equations can be reorganized into two main conditions,

$$\begin{cases} \mathcal{F}(s)[\partial_x u_1] = \mathcal{R}g\beta[P], \\ \mathcal{F}^m(s)[\partial_x u_1] = -(u_1 - s)\mathcal{R}g\beta[\partial_x Q], \end{cases} \quad (3.49)$$

which allow us to compare the precipitation front speed s with the dry and moist characteristic velocities, $\mathcal{F}(c)=0$ and $\mathcal{F}^m(c)=0$, as a function of the sign of $[\partial_x u_1]$, $[\partial_x Q]$, and $[P]$. The term \mathcal{R} is given by Eq. (3.26).

Linearization of the coefficients of the jump conditions in Eq. (3.49) around the state of rest gives

$$\begin{cases} (s^2 - C_+)(s^2 - C_-)[\partial_x u_1] = -(\alpha - 1)gH_2g\beta[P], \\ (s^2 - C_+^m)(s^2 - C_-^m)[\partial_x u_1] = -s(\alpha - 1)gH_2g\beta[\partial_x Q]. \end{cases} \quad (3.50)$$

For a configuration where condensation arises on the right side of the discontinuity, $P_- = 0$ and $P_+ = -Q^s \partial_x u_{1+} > 0$, there exist five types of precipitation fronts:

- (1) the dry external fronts, $\sqrt{C_+} < s < \sqrt{C_+^m}$,
- (2) the dry internal subsonic fronts, $\sqrt{C_-^m} < s < \sqrt{C_-}$,
- (3) the moist internal subsonic fronts, $-\sqrt{C_-^m} < s < 0$,
- (4) the moist internal supersonic fronts, $-\sqrt{C_+} < s < -\sqrt{C_-}$, and
- (5) the moist external fronts, $s < -\sqrt{C_+^m}$.

These internal fronts are exactly the precipitation fronts found by Frierson *et al.*³ in a linear baroclinic model.

Figures 5 and 6 show the nonlinear solutions s of Eq. (3.49) for the configuration $P_- = 0$ as functions of the baroclinic velocity u^{bc} for $[\partial_x u_1] < 0$ and $[\partial_x u_1] > 0$, respectively. Note that the solutions in the configuration $P_- = 0$ only exist for $s - u_1 < Q^s [\partial_x u_1] / [\partial_x Q]$. Linearized results are well verified for $u^{bc} = 0$: the precipitation fronts 1, 2, 3, and 5 are represented in Fig. 5, and the front 4 in Fig. 6. As for the characteristic velocities, the inequalities that define them are maintained for $|u^{bc}| / \sqrt{gh_1} < 1$ ($\mathcal{R} < 0$).

D. Summary of the properties of the mc2RSW model

We have shown that the mc2RSW model has enjoyable properties. In precipitating regions, the mass transfer from the lower to the upper layer induces a momentum transfer, a PV modification, and a total energy variation, which correspond to physical intuition. As it should be, the moist enthalpy (ME) in the humid lower layer is locally conserved, offering a new Lagrangian invariant: the moist potential vorticity (MPV). The system is hyperbolic for positive ME and moderate baroclinic velocities. In the immediate relaxation limit ($\tau \rightarrow 0$), the system becomes piecewise hyperbolic and moist characteristics appear in the precipitating regions. As in the observations,¹⁶ the moist internal (mostly baroclinic) characteristics propagate more slowly than the dry ones for positive moist enthalpy and moderate baroclinic velocity ($\mathcal{R} < 0$). Under these conditions, five types of precipitation front exists. Among them, the three internal ones are the two-layer equivalents of the precipitation fronts previously found in linear baroclinic³ and nonlinear one-layer¹ models.

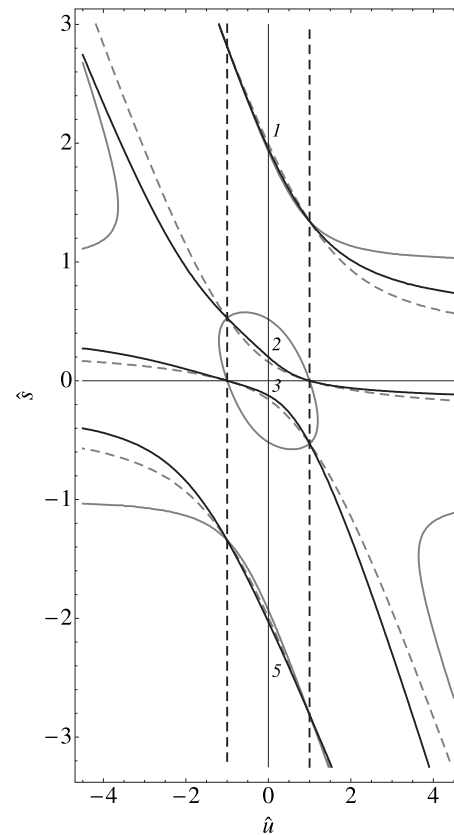


FIG. 5. Solutions $\hat{s} = s - u_1 / \sqrt{gh_1}$ of the implicit Eq. (3.49) (solid black) as functions of baroclinic velocities $\hat{u} = u^{bc} / \sqrt{gh_1}$ for the configuration with $P_- = 0$ and $[\partial_x u_1] < 0$. Solid and dashed gray lines correspond to dry and moist characteristic velocities, respectively, as in Fig. 3. Vertical dashed lines correspond to solutions of the equation $\mathcal{R} = 0$ for which the dry and moist characteristic velocities are identical: $|\hat{u}| = 1$. The nonlinear extension of precipitation fronts 1, 2, 3, and 5 of Eq. (3.50) are found for $|\hat{u}| < 1$ ($\mathcal{R} < 0$). Here, $\gamma = h_1/h_2 = 0.5$, $\alpha = 1.5$, $\beta Q^s/h_1 = 0.9$, and $\sqrt{gh_1}\beta[\partial_x Q]/h_1[\partial_x u_1] = 0.3$.

IV. THE TWO-LAYER MOIST-CONVECTIVE RSW MODEL WITH CONSTANT LOWER PRESSURE (“RIGID BOTTOM” RB-MC2RSW)

It is perfectly natural that the fast [cf. Eq. (3.29)] moist external waves appear in the two-layer system with two free

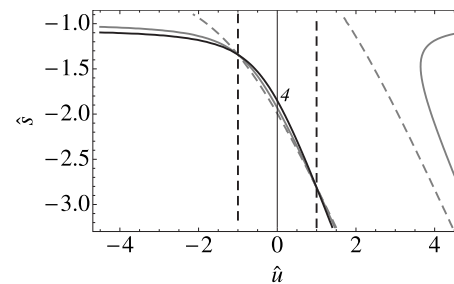


FIG. 6. Solutions $\hat{s} = s - u_1 / \sqrt{gh_1}$ of the implicit Eq. (3.49) (solid black) as functions of baroclinic velocities $\hat{u} = u^{bc} / \sqrt{gh_1}$ for the configuration with $P_- = 0$ and $[\partial_x u_1] > 0$. Solid and dashed gray lines correspond to dry and moist characteristic velocities, respectively, as in Fig. 3. Vertical dashed lines correspond to solutions of $\mathcal{R} = 0$ for which the dry and moist characteristic velocities are identical: $|\hat{u}| = 1$. The nonlinear extension of precipitation front 4 of Eq. (3.50) is found for $|\hat{u}| < 1$ ($\mathcal{R} < 0$). $\gamma = h_1/h_2 = 0.5$, $\alpha = 1.5$, $\beta Q^s/h_1 = 0.9$, and $\sqrt{gh_1}\beta[\partial_x Q]/h_1[\partial_x u_1] = -1$.

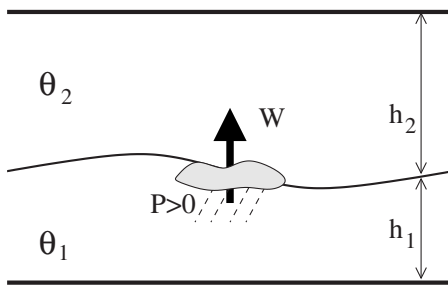


FIG. 7. Sketch of the rb-mc2RSW model.

material surfaces. However, they have no counterparts in the observations, and seem to be physically irrelevant. These waves may be easily filtered by “freezing” the lower boundary, which leads to a purely baroclinic two-layer model. We will briefly present the main properties of such a model in this section. The previously used boundary condition at z_0 is henceforth changed: the geopotential $\phi(z_0)$ is now free and z_0 is constant.

A. The model

The corresponding system, sketched in Fig. 7, is described by the following set of equations:

$$\partial_t \mathbf{v}_1 + (\mathbf{v}_1 \cdot \nabla) \mathbf{v}_1 + f \mathbf{k} \times \mathbf{v}_1 = -\nabla \phi_1, \quad (4.1)$$

$$\partial_t \mathbf{v}_2 + (\mathbf{v}_2 \cdot \nabla) \mathbf{v}_2 + f \mathbf{k} \times \mathbf{v}_2 = -\nabla \phi_2 + \frac{\mathbf{v}_1 - \mathbf{v}_2}{h_2} \beta P, \quad (4.2)$$

$$\partial_t h_1 + \nabla \cdot (h_1 \mathbf{v}_1) = -\beta P, \quad (4.3)$$

$$\partial_t h_2 + \nabla \cdot (h_2 \mathbf{v}_2) = +\beta P, \quad (4.4)$$

$$\partial_t Q + \nabla \cdot (Q \mathbf{v}_1) = -P, \quad (4.5)$$

$$\phi_2 - \phi_1 = g(h_1 + \alpha h_2), \quad (4.6)$$

where $\phi_1 = \phi(z_0)$, $\phi_2 = \phi(z_2)$, and $\alpha = \theta_2 / \theta_1$ as before. Due to the constraint

$$h_1 + h_2 = H = \text{const}, \quad (4.7)$$

the only independent height variable is the deviation of the interface from its rest position. As usual, in the rigid lid/bottom two-layer RSW,²⁴ the barotropic part of the geopotential is not an independent variable and may be expressed, up to an arbitrary function of time, in terms of other variables via the constraint

$$\nabla \cdot \frac{\mathbf{v}_1 h_1 + \mathbf{v}_2 h_2}{H} = 0. \quad (4.8)$$

The baroclinic part of the pressure is then determined from the dynamic boundary condition at the interface [Eq. (4.6)].

B. Conservation laws

The conservation laws for moist enthalpy, PV and MPV, are the same as in the mc2RSW model, cf. Sec. II. Using Eqs. (4.7) and (4.8), one can show that the evolution of the

total energy of the isolated system is the same as in the mc2RSW model, and is given by Eq. (3.8). Momentum equations are identical to Eqs. (3.10) and (3.11), except for the two first terms in the rhs, which are replaced by $-h_1 \nabla \phi_1$ and $-h_2 \nabla \phi_2$ for the lower and the upper layer equations, respectively. As in the mc2RSW model, the total momentum is locally conserved in the absence of rotation ($f=0$).

C. Mathematical properties

1. Characteristic equation

In order to reduce the 1.5D version of the system [Eqs. (4.1)–(4.7)] with all dependence on y removed to the quasi-linear form Eq. (3.15), an additional hypothesis is required to fix the barotropic component of the geopotential. For simplicity, we set the barotropic velocity in the x direction to be zero: $u^{bt} = (u_1 h_1 + u_2 h_2) / H = 0$. Since H is constant, this hypothesis means that the total barotropic momentum in the x direction is zero. This allows us to determine the derivative of the geopotential ϕ_1 as a function of other variables,²⁴

$$\partial_x \phi_1 = \frac{1}{H} \left\{ -\partial_x \left(u_1^2 h_1 + u_2^2 h_2 + g(\alpha - 1) \frac{h_2^2}{2} \right) + f(v_1 h_1 + v_2 h_2) \right\}. \quad (4.9)$$

The propagating solutions of the characteristic equation of the reduced 1.5D system obtained in this way

$$c_{\pm} = \frac{u_1 h_2 + u_2 h_1}{H} \pm \sqrt{\frac{h_1 h_2}{H^2} \Upsilon}, \quad (4.10)$$

and are real if $\Upsilon = g(\alpha - 1)H - (u_1 - u_2)^2 \geq 0$. Linearizing this equation, one obtains

$$c_d = \sqrt{g(\alpha - 1)H_e}, \quad (4.11)$$

where $H_e = H_1 H_2 / H$ is the equivalent height and $g(\alpha - 1)$ is the reduced gravity.

In the immediate relaxation approximation ($\tau \rightarrow 0$), the system [Eqs. (4.1)–(4.6)] can be rewritten in the precipitating regions, where $P = -Q^s \nabla \cdot \mathbf{v}_1$, as follows:

$$\begin{cases} \partial_t \mathbf{v}_1 + (\mathbf{v}_1 \cdot \nabla) \mathbf{v}_1 + f \mathbf{k} \times \mathbf{v}_1 = -\nabla \phi_1, \\ \partial_t \mathbf{v}_2 + (\mathbf{v}_2 \cdot \nabla) \mathbf{v}_2 + f \mathbf{k} \times \mathbf{v}_2 = -\nabla \phi_2 - \frac{\mathbf{v}_1 - \mathbf{v}_2}{h_2} \beta Q^s \nabla \cdot \mathbf{v}_1, \\ \partial_t h_1 + \nabla \cdot (h_1 \mathbf{v}_1) = +\beta Q^s \nabla \cdot \mathbf{v}_1, \\ \partial_t h_2 + \nabla \cdot (h_2 \mathbf{v}_2) = -\beta Q^s \nabla \cdot \mathbf{v}_1, \\ \phi_2 - \phi_1 = g(h_1 + \alpha h_2). \end{cases} \quad (4.12)$$

Under the same hypothesis of zero barotropic velocity for the 1.5D version of the system [Eq. (4.12)], the propagating characteristics c_{\pm}^m have the same expression as Eq. (4.10) with the discriminant Υ replaced by

$$\begin{aligned}
Y^m &= g(\alpha - 1)H \left(1 - \frac{\beta Q^s}{h_1}\right) - (u_1 - u_2)^2 \left(1 - \frac{\beta Q^s H}{h_1 h_2}\right) \\
&= Y + \mathcal{R} \frac{\beta Q^s H}{h_1 h_2},
\end{aligned}
\tag{4.13}$$

where the coefficient \mathcal{R} is given in Eq. (3.26). One observes that these moist characteristics are real and the hyperbolicity in the precipitating regions is guaranteed if $Y^m \geq 0$. Moreover, these characteristics propagate more slowly than the dry ones if $\mathcal{R} < 0$. For the linearized 1.5D version of the system [Eq. (4.12)], one finds

$$c_m = c_d \sqrt{1 - \frac{\beta Q^s}{H_1}} < c_d, \tag{4.14}$$

if the moist enthalpy in the state of rest is positive: $M_1 = H_1 - \beta Q^s > 0$.

2. Criterion of hyperbolicity

The criterion of hyperbolicity becomes explicit and is based on the positivity of the discriminant of the characteristic velocities. In the nonprecipitating regions, $Y \geq 0$ if the vertical shear satisfies the condition

$$\frac{|u^{bc}|}{\sqrt{gH}} \leq \sqrt{\alpha - 1}. \tag{4.15}$$

This condition is analogous to the one found in Ref. 24 in the two-layer model of the ocean, and corresponds to the threshold of the Kelvin–Helmholtz (KH) instability, a classical ageostrophic instability arising in shear flows.

In precipitating regions in the immediate relaxation limit ($\tau \rightarrow 0$), $Y^m \geq 0$ replaces the previous condition and the criterion becomes

$$\frac{|u^{bc}|}{\sqrt{gH}} \leq \sqrt{(\alpha - 1) \frac{1 - \frac{\beta Q^s}{h_1}}{1 - \frac{\beta Q^s}{h_e}}}, \tag{4.16}$$

where $h_e = h_1 h_2 / H$ is the equivalent height and the moist enthalpy is supposed to be positive: $m_1 = h_1 - \beta Q^s > 0$. This shows that the hyperbolicity is easier to preserve in the precipitating regions since $h_e < h_1$. Furthermore, $Y^m \geq 0$ is immediately satisfied if $h_e \leq \beta Q^s$.

3. Linearized Riemann variables

Even if the solutions of the nonlinear characteristic equation are known analytically, cf. Eq. (4.10), the associated Riemann variables are not. A linearization, following the lines of Sec. III C 3, is then used for the system [Eqs. (4.1)–(4.6)]. Under the hypothesis of zero zonal barotropic velocity, and in the absence of rotation, one obtains

$$\begin{cases}
(\partial_t \pm c_d \partial_x) r_{\pm} = \mp \frac{c_d}{H_1} \beta P, \\
\partial_t r_0 = - \left(1 - \frac{\beta \bar{Q}}{H_1}\right) P.
\end{cases}
\tag{4.17}$$

Similarly to the mc2RSW model, the linearized Riemann variables

$$\begin{cases}
r_{\pm} = u_1 \pm \frac{c_d}{H_1} \eta_1, \\
r_0 = Q - \frac{\bar{Q}}{H_1} \eta_1,
\end{cases}
\tag{4.18}$$

are modified in precipitating regions. In the immediate relaxation approximation ($\tau \rightarrow 0$), the moist Riemann variables

$$r_{\pm}^m = u_1 \pm \frac{c_m}{M_1} \eta_1 \tag{4.19}$$

defined in the precipitating regions are invariant.

4. Fronts and Rankine–Hugoniot conditions

a. Strong discontinuities: Shocks. The RH conditions for a strong shock [Eq. (3.45)] or a strong shock inside a precipitating region in the immediate relaxation limit [Eq. (3.46)] still hold with the replacement of the first condition in Eq. (3.45) by

$$\left[u_1^2 h_1 + u_2^2 h_2 + g(\alpha - 1) \frac{h_2^2}{2} + H \phi_1 \right] = 0, \tag{4.20}$$

which satisfies the condition of zero barotropic zonal velocity $u_1 h_1 + u_2 h_2 = 0$ through the shock.

b. Precipitation fronts. The RH conditions [Eq. (3.48)] corresponding to precipitation fronts in the 1.5D mc2RSW model still hold, except for the two first conditions, which must be replaced by the unique condition

$$(u_1 - s)[\partial_x u_1] + [\partial_x \phi_1] = 0, \tag{4.21}$$

where $\partial_x \phi_1$ is given in Eq. (4.9). These can be combined into two main conditions:

$$\begin{cases}
(s - c_+)(s - c_-)[\partial_x u_1] = -\frac{1}{H} \mathcal{R} \beta [P], \\
(s - c_+^m)(s - c_-^m)[\partial_x u_1] = \frac{1}{H} (u_1 - s) \mathcal{R} \beta [\partial_x Q].
\end{cases}
\tag{4.22}$$

For $\mathcal{R} < 0$, the hyperbolicity is preserved everywhere ($Y > Y^m > 0$) and the moist characteristic velocities are slower than the dry ones: $|c_{\pm}^m| < |c_{\pm}|$. Defining the velocities relative to the velocity in the lower layer $\hat{c} = c - u_1$ (and $\hat{s} = s - u_1$), one can show that

$$\hat{c}_- < \hat{c}_-^m < 0 < \hat{c}_+^m < \hat{c}_+, \tag{4.23}$$

where baroclinic zonal velocity $u^{bc} = u_1 - u_2 < 0$ is chosen to be negative. Consequently, for the configuration $[P] > 0$ and $[\partial_x Q] < 0$, three precipitation fronts are found,

- (1) the dry subsonic fronts, $\hat{c}_+^m < \hat{s} < \hat{c}_+$,
- (2) the moist subsonic fronts, $\hat{c}_-^m < \hat{s} < 0$, and
- (3) the moist supersonic fronts, $\hat{s} < \hat{c}_-$.

They are equivalent to the ones obtained in the one-layer model.¹ In the case of positive baroclinic zonal velocity $u^{bc} > 0$, the relation [Eq. (4.23)] is reversed and the same precipitation fronts are found with subscripts + and - interchanged. Note that the case $\mathcal{R} > 0$ should be discarded, even if hyperbolicity is preserved with $Y^m > Y > 0$, because it allows the moist characteristics to propagate faster than the dry ones, which is unphysical.

D. Summary of the properties of the rb-mc2RSW model

Thus, the rigid bottom mc2RSW (rb-mc2RSW) model filters out the external characteristics while preserving all other properties of the mc2RSW model. It provides a nonlinear equivalent of the linear model previously studied in Refs. 2–5. Note, however, that the rigid bottom/lid boundary conditions are more difficult to treat by the finite-volume numerical methods than the free-surface ones (see Sec. VI below).

V. LIMITING EQUATIONS AND RELATION TO THE KNOWN MODELS

A. Formulation in terms of the barotropic and baroclinic components

We first explicitly formulate the two-layer model in its generic setting [Eqs. (2.9), (2.10), and (2.13)] in terms of barotropic and baroclinic components, in order to see how each component is affected by precipitation and moist convection.

The baroclinic-barotropic decomposition of the velocity field is defined by

$$\begin{cases} \mathbf{v}^{bt} = \frac{h_1 \mathbf{v}_1 + h_2 \mathbf{v}_2}{h_1 + h_2}, \\ \mathbf{v}^{bc} = \mathbf{v}_1 - \mathbf{v}_2, \end{cases} \Rightarrow \begin{cases} \mathbf{v}_1 = \mathbf{v}^{bt} + \left(1 - \frac{h}{H}\right) \mathbf{v}^{bc}, \\ \mathbf{v}_2 = \mathbf{v}^{bt} - \frac{h}{H} \mathbf{v}^{bc}, \end{cases} \quad (5.1)$$

where $H = h_1 + h_2$ and $h_1 = h$ hereafter. For a dry upper layer, $Q_2 = 0$, $q(z_2) = 0$, and $P_2 = 0$, and mass and moisture conservation equations become

$$\partial_t H + \nabla \cdot (H \mathbf{v}^{bt}) = -W_2, \quad (5.2)$$

and

$$\begin{cases} \partial_t h + \nabla \cdot \left(h \left\{ \mathbf{v}^{bt} + \left(1 - \frac{h}{H}\right) \mathbf{v}^{bc} \right\} \right) = -W_1, \\ \partial_t Q + \nabla \cdot \left(Q \left\{ \mathbf{v}^{bt} + \left(1 - \frac{h}{H}\right) \mathbf{v}^{bc} \right\} \right) = -P. \end{cases} \quad (5.3)$$

The momentum equations contain double (K^{bc-bc} , G^{bt-bt} , G^{bc-bc}) and mixed (K^{bt-bc}) terms that describe the self-interaction of the barotropic and the baroclinic modes, and their nonlinear coupling, respectively,

$$\begin{aligned} \partial_t \mathbf{v}^{bt} + f \mathbf{k} \times \mathbf{v}^{bt} + G^{bt-bt} + G^{bc-bc} \\ = -\frac{h}{H} \{ \nabla \phi(z_1) - g \nabla z_1 \} \\ - \left(1 - \frac{h}{H} \right) \{ \nabla \phi(z_2) - \alpha g \nabla z_2 \} + \frac{h \mathbf{v}^{bc}}{H^2} W_2, \end{aligned} \quad (5.4)$$

$$\begin{aligned} \partial_t \mathbf{v}^{bc} + f \mathbf{k} \times \mathbf{v}^{bc} + K^{bc-bc} + K^{bt-bc} \\ = -g(\alpha - 1) \nabla (h - H) + \frac{\mathbf{v}^{bc}}{H - h} W_1. \end{aligned} \quad (5.5)$$

The precise form of the (rather cumbersome) terms K^{bc-bc} , G^{bt-bt} , G^{bc-bc} , and K^{bt-bc} , which are easy to write down, is not important at the moment.

As expected, if $W_2 = 0$, as in the above-considered mc2RSW and rb-mc2RSW models, the terms $W_1 = \beta P$ directly influence the baroclinic components (\mathbf{v}^{bc} , h) in the precipitating regions ($P > 0$). This is in agreement with the observations, which indicate that moist convection mostly affects the baroclinic motions in the troposphere.

Based on this observation, purely baroclinic dynamics is often considered in the literature.³ With a constant total height H and no convection at the upper surface $W_2 = 0$ (rb-mc2RSW model), the barotropic velocity becomes nondivergent, see Eq. (5.2), and, for small perturbations around the state of rest ($h = H_1 + \eta$), \mathbf{v}^{bt} is indeed decoupled from \mathbf{v}^{bc} , being forced only by $\nabla \phi(z_0)$. Note that the last term of the \mathbf{v}^{bc} Eq. (5.5) should not be taken into account, since it is of the second-order of perturbation in the precipitating regions ($P > 0$). The resulting linear system in the baroclinic sector coincides with models previously studied in the literature^{2–5} for $\eta \equiv -\theta$,

$$\begin{cases} \partial_t \mathbf{v}^{bc} + f \mathbf{k} \times \mathbf{v}^{bc} = -g_e \nabla \eta, \\ \partial_t \eta + H_e \nabla \cdot \mathbf{v}^{bc} = -\beta P, \\ \partial_t Q + Q_e \nabla \cdot \mathbf{v}^{bc} = -P, \end{cases} \quad (5.6)$$

where $g_e = g(\alpha - 1)$ and $Q_e = (H_e / H_1) Q^s$.

However, the nonlinearity couples barotropic and baroclinic components and produces an indirect influence of the precipitation over the former. Note, finally, that if $W_2 \neq 0$ (see Appendix A), the barotropic component is directly affected by the moist processes but the system in this case should be considered as the lower part of a more general three-layer system.

B. Quasigeostrophic approximation

Needless to say, the quasigeostrophic (QG) approximation resulting from the full “primitive” equations in the limit of small Rossby numbers is relevant for large-scale atmospheric motions that are, generally, close to the geostrophic equilibrium in temperate latitudes. This approximation for the multilayer RSW equations may be systematically derived by multiscale asymptotic expansions,²⁵ with different QG regimes arising for different aspect ratios and strong/weak nonlinearity. Below, we will limit ourselves to the standard QG regime²⁶ with typical nonlinearity of the order of the Rossby number, and the unperturbed thicknesses of the layers of the

same order. In the mc2RSW model, we introduce a (single) characteristic length scale L , a characteristic velocity scale V , and the vortex turnover time-scale $T=L/V$, and define the barotropic deformation radius $R_d=\sqrt{gH}/f_0$, where $H=H_1+H_2$ is the total height at the state of rest. The nondimensional thicknesses of the layers are $D_i=H_i/H_0$, and will be supposed to be of the same order. Dimensionless parameters of the system, thus, are the Rossby number $\epsilon=V/f_0L$, the barotropic Burger number $s^{bt}=R_d^2/L^2$, the typical nondimensional deviation of the interface (and the free surface) λ , and the nondimensional gradient of the Coriolis parameter β/L , where $f=f_0+\beta y$. We then make a standard QG hypothesis $\epsilon\sim\lambda\sim\beta/f_0L\rightarrow 0$, with $s^{bt}\sim O(1)$. We will consider a quasi-saturated state for which the deviations from the saturation will be supposed to be small and of the same order as other small parameters $Q=H_0(Q^s+\epsilon q)$. The nondimensional mc2RSW equations are then given by

$$\left\{ \begin{aligned} \epsilon\{\partial_t \mathbf{v}_1 + (\mathbf{v}_1 \cdot \nabla) \mathbf{v}_1\} + (1 + \epsilon y) \mathbf{k} \times \mathbf{v}_1 &= -\nabla(\eta_1 + \eta_2), \\ \epsilon\{\partial_t \mathbf{v}_2 + (\mathbf{v}_2 \cdot \nabla) \mathbf{v}_2\} + (1 + \epsilon y) \mathbf{k} \times \mathbf{v}_2 \\ &= -\nabla(\eta_1 + \alpha \eta_2) + \epsilon^2 \frac{\mathbf{v}_1 - \mathbf{v}_2}{D_2 + \epsilon \eta_2} W_1, \\ \epsilon \partial_t \eta_1 + \nabla \cdot \{(D_1 + \epsilon \eta_1) \boldsymbol{\epsilon}_1\} &= -\epsilon W_1, \\ \epsilon \partial_t \eta_2 + \nabla \cdot \{(D_2 + \epsilon \eta_2) \boldsymbol{\epsilon}_2\} &= -\epsilon(W_2 - W_1), \\ \epsilon \partial_t q + \nabla \cdot \{(Q^s + \epsilon q) \boldsymbol{\epsilon}_1\} &= -\epsilon P. \end{aligned} \right. \quad (5.7)$$

The QG approximation, as usual, is obtained by retaining the first two orders in the asymptotic expansion of the velocity field in Rossby number $\mathbf{v}_i = \sum_j \epsilon^j \mathbf{v}_i^{(j)}$. The geostrophic equilibrium appears at $O(\epsilon^0)$,

$$\mathbf{k} \times \mathbf{v}_i^{(0)} = -\nabla \psi_i, \quad (5.8)$$

where ψ_i is the geostrophic streamfunctions defined by

$$\left\{ \begin{aligned} \psi_1 &= \eta_1 + \eta_2, \\ \psi_2 &= \eta_1 + \alpha \eta_2. \end{aligned} \right. \quad (5.9)$$

The evolution of the nondivergent geostrophic velocity field is obtained at $O(\epsilon^1)$,

$$\frac{d_1^{(0)}}{dt} \left(\nabla^2 \psi_1 + y - \frac{\eta_1}{D_1} \right) = \frac{W_1}{D_1}, \quad (5.10)$$

$$\frac{d_2^{(0)}}{dt} \left(\nabla^2 \psi_2 + y - \frac{\eta_2}{D_2} \right) = \frac{W_2 - W_1}{D_2}, \quad (5.11)$$

where $d_i^{(0)}/dt = \partial_t + (\mathbf{v}_i^{(0)} \cdot \nabla)$ represents advection by the geostrophic velocity field. Equations (5.10) and (5.11) express the PV conservation in the lower and upper layers, respectively. The moisture conservation at $O(\epsilon^1)$ can be combined with Eq. (5.10) with $W_1 = \beta P$ to express the moist potential vorticity conservation in the lower layer,

$$\frac{d_1^{(0)}}{dt} \left(\nabla^2 \psi_1 + y - \frac{\eta_1 - \beta q}{D_1 - \beta Q^s} \right) = 0. \quad (5.12)$$

For the rb-mc2RSW model under the QG assumptions, the same equations result, with a change of the barotropic by the baroclinic Burger number s^{bc} , where the baroclinic deformation radius is defined as $R_d = \sqrt{g(\alpha-1)H_0}/f$. The geostrophic streamfunctions coincide with geopotentials: $\psi_i = \phi_i$, and are expressed in terms of the interface displacement by $\eta = \eta_1 = -\eta_2$. This latter case is strictly equivalent to the model used in Ref. 6 if dissipation and friction are neglected, with the same expressions for the coefficients β_i , cf. Eq. (2.16).

Note that the QG Eqs. (5.10) and (5.11) may be directly derived as the QG approximation of the PV Eqs. (3.12)–(3.14) in the mc2RSW and rb-mc2RSW models.

C. Reduced gravity model: Another justification of the mcRSW model

In this section, we present another way to derive the mcRSW model introduced in a previous work¹ starting from the two-layer mc2RSW model. We consider the following characteristic length scale:

$$L = \sqrt{g^* H_e} T, \quad (5.13)$$

where $g^* = g(\alpha-1)/\alpha$ is the reduced gravity, $H_e = H_1 H_2 / H_0$ is the equivalent height, and $H_0 = H_1 + H_2$ is the total height at rest. We assume that the upper layer is almost at rest and is much thicker than the lower one, so that we can introduce the following small parameter:

$$\epsilon = \frac{H_1}{H_0} = 1 - \frac{H_2}{H_0} \ll 1. \quad (5.14)$$

The typical velocities in the respective layers are as follows:

$$U_1 = (1 - \epsilon) \sqrt{g^* H_e} \quad \text{and} \quad U_2 = \epsilon \sqrt{g^* H_e}. \quad (5.15)$$

Finally, we express the heights h_1 and h_2 as functions of the dimensionless interface and lower surface displacements,

$$\frac{h_2}{H_2} = 1 + \epsilon h^* \quad \text{and} \quad \frac{h_1 + h_2}{H_0} = 1 + \epsilon \frac{g^* H_2^2}{g H_0^2} \eta. \quad (5.16)$$

Note that the scale of Q is $H_1 = \epsilon H_0$, as it is concentrated in the lower layer.

Using this scaling, the mc2RSW model Eqs. (3.1)–(3.5) take the following dimensionless form:

$$\left\{ \begin{array}{l} \partial_t \mathbf{v}_1 + (1 - \epsilon)(\mathbf{v}_1 \cdot \nabla) \mathbf{v}_1 + f \mathbf{k} \times \mathbf{v}_1 = -\nabla \eta, \\ \epsilon \partial_t \mathbf{v}_2 + \epsilon^2 (\mathbf{v}_2 \cdot \nabla) \mathbf{v}_2 + \epsilon f \mathbf{k} \times \mathbf{v}_2 = -\alpha \nabla h^* - (1 - \epsilon) \nabla \eta + \frac{\epsilon}{1 - \epsilon} \frac{(1 - \epsilon) \mathbf{v}_1 - \epsilon \mathbf{v}_2}{1 + \epsilon h^*} \beta P, \\ \partial_t \left\{ \frac{\alpha - 1}{\alpha} (1 - \epsilon) \eta - h^* \right\} + \nabla \cdot \left\{ \mathbf{v}_1 \left(1 + (1 - \epsilon) \left\{ \frac{\alpha - 1}{\alpha} (1 - \epsilon)^2 \eta - h^* \right\} \right) \right\} = -\frac{1}{1 - \epsilon} \beta P, \\ \partial_t h^* + \nabla \cdot \{ \mathbf{v}_2 (1 + \epsilon h^*) \} = +\frac{1}{1 - \epsilon} \beta P, \\ \partial_t Q + (1 - \epsilon) \nabla \cdot (Q \mathbf{v}_1) = -P. \end{array} \right. \quad (5.17)$$

In the limit $\epsilon \rightarrow 0$, this system is reduced to

$$\left\{ \begin{array}{l} \partial_t \mathbf{v}_1 + (\mathbf{v}_1 \cdot \nabla) \mathbf{v}_1 + f \mathbf{k} \times \mathbf{v}_1 = -\nabla \eta, \\ \partial_t \eta + \nabla \cdot \{ \mathbf{v}_1 (1 + \eta) \} = -\beta P, \\ \partial_t Q + \nabla \cdot (Q \mathbf{v}_1) = -P, \end{array} \right. \quad (5.18)$$

if we assume that $\eta + \alpha h^* = 0$ is constant. Consequently, the velocity \mathbf{v}_2 is expressed in terms of other variables via

$$\nabla \cdot \mathbf{v}_p = \nabla \cdot \{ \mathbf{v}_1 (1 + \eta) + \alpha \mathbf{v}_2 \} = (\alpha - 1) \beta P, \quad (5.19)$$

where \mathbf{v}_p is “pseudobarotropic” velocity, which is nondivergent in the nonprecipitating regions. This condition is standard²⁷ in the derivation of the reduced gravity model for the ocean, where the gradient of the geopotential at the upper surface is cancelled $\nabla \phi(z_2) = 0$.

The system [Eq. (5.18)] is the dimensionless mcRSW model of Bouchut *et al.*,¹ and we thus demonstrated that it is directly related to the “parent” two-layer model. Note that this result is also valid for the two-layer mcRSW model with nonzero convective flux through the upper boundary derived in Appendix A, but the condition [Eq. (5.19)] should be replaced by $\nabla \cdot \mathbf{v}_p = -\beta P$.

VI. NUMERICAL ILLUSTRATIONS

We present here two numerical experiments with a high-resolution shock-capturing finite-volume code. The purpose of the first is to benchmark the numerical scheme by comparing with one-layer simulations, and to illustrate the results obtained in the previous sections, in particular for fronts and shocks. Therefore, the setup is chosen deliberately the same as in the experiments with the one-layer model of Ref. 1. The second experiment gives an example of a fully baroclinic phenomenon, and illustrates the capability of the code to resolve the fine details of the dynamics. We perform simulations in the framework of the 1D nonrotating version of the full mc2RSW model, without making the rb-mc2RSW re-

duction. Numerically, it is easier to treat the first than the second, because of the incompressibility constraint for the barotropic velocity in the latter.

A. Numerical scheme

There are additional numerical problems in the two-layer RSW model, even in its dry version, as compared to the one-layer RSW model. First, two-layer RSW can be nonhyperbolic and have complex characteristic velocities, see Secs. III C 1 and III C 2. Second, as mentioned in Secs. III B and III C 4, the system is not fully conservative, which implies a lack of appropriate RH relations. This latter difficulty was largely discussed in Ref. 15.

A robust well balanced finite-volume scheme for the multilayer shallow-water system was proposed in Ref. 28. The first tests in the oceanic context demonstrated its efficiency.²⁹ At each timestep, the scheme uses a one-layer hydrostatic reconstruction solver for each layer. It then modifies the resulting numerical fluxes to preserve the total momentum conservation. The centered discretization used in the scheme is consistent with the momentum conservation in each layer. Note that this property is common with an older scheme by Castro *et al.*³⁰ More details can be found in Ref. 28. Rotation and transverse velocity may be introduced as in the one-layer system,³¹ and the equation of the conserved tracer Q is added. The precipitation is introduced as conditional source/sink switched at the end of each iteration, see Appendix C of Ref. 1. This scheme does not support the rigid lid constraint, and thus is only applicable to the mc2RSW model (or the ml-mc2RSW model presented in Appendix A).

Since the original construction of Ref. 28 corresponds to the standard “oceanic” configuration and uses densities $\rho_{1,2}$ and the free upper surface, an appropriate change of variables has to be performed for the input and output variables in order to adapt it to the atmospheric configuration, see Table I.

B. Choice of parameters

The scale of the domain is fixed at $L_x \times L_y = 10 \times 10$ in the units of length L . Since there is no intrinsic horizontal scale in the model in the absence of rotation, the length scale is $L = \sqrt{g H_0 T}$, where H_0 is the sum of the layer thicknesses at rest and T is the time-scale.

TABLE I. Correspondence between atmospheric and oceanic two-layer shallow-water variables.

Atmosphere	h_1	h_2	\mathbf{v}_1	\mathbf{v}_2	θ_1 / θ_0	θ_2 / θ_0	$\phi(z_0)$
Ocean	$\rho_2 h_2$	$\rho_1 h_1$	\mathbf{v}_2	\mathbf{v}_1	$1 / \rho_2$	$1 / \rho_1$	$g z_0$

TABLE II. Parameter values in numerical simulations.

H_0	$\alpha = \theta_2 / \theta_1$	Q^s	β
3	1.5	0.9	1

We choose a high resolution in the zonal direction x with $n_x=500$ grid points. The timestep is chosen as the minimum between a specific value allowing to respect the Courant–Friedrich–Levy (CFL) condition, Δt^{CFL} , and some maximum value Δt^{\max} (which was chosen to be $\pi/5$).

Neumann boundary conditions are numerically implemented by requiring that each variable has the same values in the two first and two last cells of the domain. Even if these conditions do not forbid complex reflections of the solutions and numerical dissipation at the boundaries, these effects are weak far from the boundaries and do not significantly affect our simulations.

The relaxation time is linked to the timestep of the numerical scheme, $\tau=5\Delta t$, and corresponds to a rapid (quasi-immediate) relaxation. The values of other parameters are given in Table II. The values chosen for β and Q^s allow us to have $\sqrt{C_-^m} \approx 0.3\sqrt{C_-}$ for $H_1=1$, for the internal moist characteristic velocity, as in the observations.¹⁶ They also correspond to the values used by Majda and collaborators in their numerical experiments.³

C. Scattering of an internal simple wave on a stationary moisture front

We first perform an experiment that benchmarks our numerical model through a direct comparison with the analytical results on the characteristics and precipitating fronts presented above, as well as with the one-layer mcRSW simulations of Ref. 1. It consists of scattering of an unidirectional propagating “simple wave” of small amplitude at a stationary moisture front.

The simple wave is a solution propagating along a single characteristic curve. It is obtained by canceling the Riemann variables on all the other characteristics. We consider an internal linear wave initially centered at $x_p=2$ and moving eastward,

$$u_1(x,0) = \begin{cases} \sigma(x-x_p)^2 + U_0 & \text{if } -\sqrt{\frac{U_0}{\sigma}} \leq x-x_p \leq \sqrt{\frac{U_0}{\sigma}}, \\ 0 & \text{otherwise,} \end{cases} \quad (6.1)$$

where $U_0=0.01$ and $\sigma=-1$. The choice of an internal simple wave maximizes the projection onto the baroclinic mode [cf. Eq. (5.1)], as compared to a simple wave propagating along the external characteristics. It is motivated by the fact that it is the baroclinic mode that is mainly affected by moist processes in the atmosphere. From the results of Sec. III C 3, one obtains the following expressions for the remaining variables:

$$\begin{cases} \eta_1(x,0) = \frac{H_1}{\sqrt{C_-}} u_1(x,0), \\ u_2(x,0) = -\left(\frac{C_+}{gH_1} - 1\right)^{-1} u_1(x,0), \\ \eta_2(x,0) = -\frac{H_2}{\sqrt{C_-}} \left(\frac{C_+}{gH_1} - 1\right)^{-1} u_1(x,0), \end{cases} \quad (6.2)$$

where the lower layer height at rest is fixed at $H_1=1$. For our choice of parameters, the external and internal linear characteristic velocities [Eq. (3.19)] are given by $\sqrt{C_+}=1.93$ and $\sqrt{C_-}=0.52$, respectively.

The stationary moisture front is placed in the middle of the domain ($x_M=5$), with the saturated area at the eastern side ($x \geq x_M$) and the unsaturated area at the western side ($x < x_M$),

$$Q(x,0) = Q^s \{1 + q_0 \tanh(x-x_M)H(-x+x_M)\}, \quad (6.3)$$

with $q_0=0.05$. The simple wave comes from the unsaturated area ($x_p < x_M$). Since it has a strong convergence at its eastern side in the lower layer ($\partial_x u_1 < 0$), it will first increase the moisture field Q on its way such that precipitation will be triggered near the moisture front.

The Hovmöller (characteristic) diagrams of the barotropic u^{bt} and baroclinic u^{bc} velocities are presented in Figs. 8(a) and 8(b), respectively. The simple wave appears in both fields and, as expected, follows the eastward internal characteristic with $\sqrt{C_-} \approx 0.5$, as long as precipitation does not occur (for $t < 4.8$). Note that some small perturbations emerge from the initial location of the wave, since the simple wave is not a solution of the full system, but only of its linearized version. Even though they are reflected at the boundaries ($t \approx 4$), the influence of these parasite perturbations remains weak.

The initial moisture field is modified by the divergence in the lower layer ($\partial_x u_1$), as shown in Fig. 8(c). A negative moisture anomaly appears once the simple wave leaves its initial position, and persists during the simulation following the nonpropagating characteristic ($c_0=0$) via the associated linearized Riemann invariant r_0 given by Eq. (3.42). Since the propagating disturbance is symmetric, it also produces a moisture anomaly on its way. Consequently, this positive anomaly follows the internal characteristic until it triggers precipitation near the moisture front.

As follows from Eq. (3.41), precipitation modifies the Riemann variables over all the characteristics. This is shown in Figs. 8(a) and 8(b) for $4.8 < t < 7.2$. In the barotropic field, the wave is partially transmitted in the saturated region as a positive anomaly along the eastward external characteristic ($\sqrt{C_+} \approx 2$). It is also partially reflected back to the unsaturated region as a positive(negative) anomaly following the internal(external) characteristics. In the baroclinic field, the anomalies on the external characteristics are too weak and only the internal reflected wave is clearly observed. This result is in full agreement with Fig. 2 of Ref. 1 in the one-layer mcRSW model.

Figure 8(c) shows that the scattering of the wave affects the moisture profile. The resulting westward internal wave

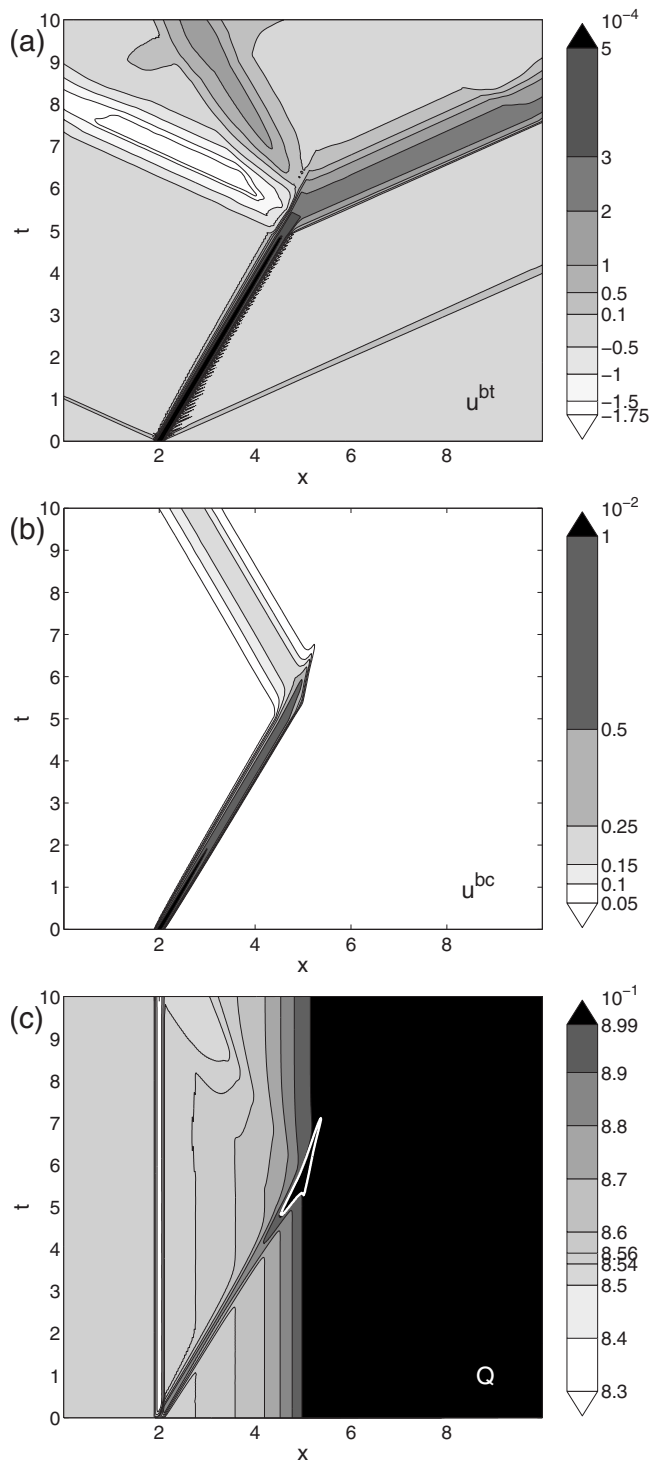


FIG. 8. Hovmöller (characteristic) diagrams of the barotropic u^{bt} (a) and baroclinic u^{bc} (b) velocities, and of the moisture field Q (c). The precipitating region is delimited by the thick white contour on panel c.

produces a weak negative anomaly of moisture on its way, while the moisture front is smoothed and displaced eastward.

The total (dry) energy of the system is well conserved as long as precipitation does not occur, as shown in Fig. 9. The energy in the lower layer is diminished by precipitation, as in the one-layer mcRSW model, see Fig. 4 in Ref. 1. This is essentially due to the convective mass loss. In compensation,

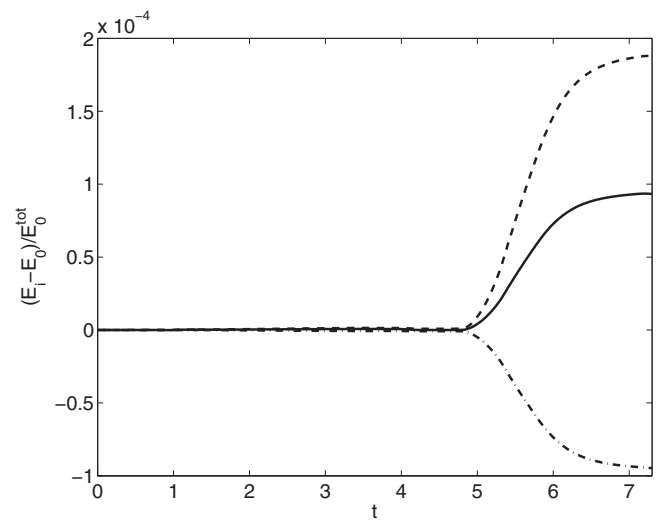


FIG. 9. Evolution of the normalized total energy in the lower layer E_1 (dashed-dotted), in the upper layer E_2 (dashed), and in the whole system E_{tot} (solid).

energy and mass in the upper layer increase. As expected from Eq. (3.8), the total energy of the system also increases. Note that the energy balance is affected by dissipation at the boundaries starting from $t \approx 7$.

In the precipitating region delimited by the thick contour in Fig. 8(c), the approach based on linearization still holds in the immediate relaxation limit ($\tau \rightarrow 0$), and the moist linearized Riemann variables [Eq. (3.44)] can be observed. Figures 10 and 11 show the Hovmöller (characteristic) diagrams of the dry and moist linearized Riemann variables in the precipitating region and its vicinity. One sees that the dry Riemann variables are indeed modified following Eq. (3.41), rewritten as

$$\begin{cases} (\partial_t \pm \sqrt{C_-} \partial_x) r_{i\pm} \propto \mp \beta P, \\ (\partial_t \pm \sqrt{C_+} \partial_x) r_{e\pm} \propto \pm \beta P. \end{cases} \quad (6.4)$$

One also checks that the values of the moist characteristic velocities correspond to the analytical results [Eq. (3.27)]

$$\begin{cases} \sqrt{C_-^m} = 0.16 < \sqrt{C_-} = 0.52, \\ \sqrt{C_+^m} = 1.99 > \sqrt{C_+} = 1.93, \end{cases} \quad (6.5)$$

by following the slopes formed by moist linearized Riemann invariants inside the precipitating region. Finally, one observes that the precipitating region is delimited by two precipitation fronts, which correspond to a dry internal subsonic front ($\sqrt{C_-^m} < s_1 < \sqrt{C_-}$) and a moist internal supersonic front ($\sqrt{C_-} < s_2 < \sqrt{C_+}$).

Alternative results are found for a simulation with the alternative model presented in Appendix A (not shown). It should be stressed that in this case the energy is always dissipated by precipitation, see Eq. (A6).

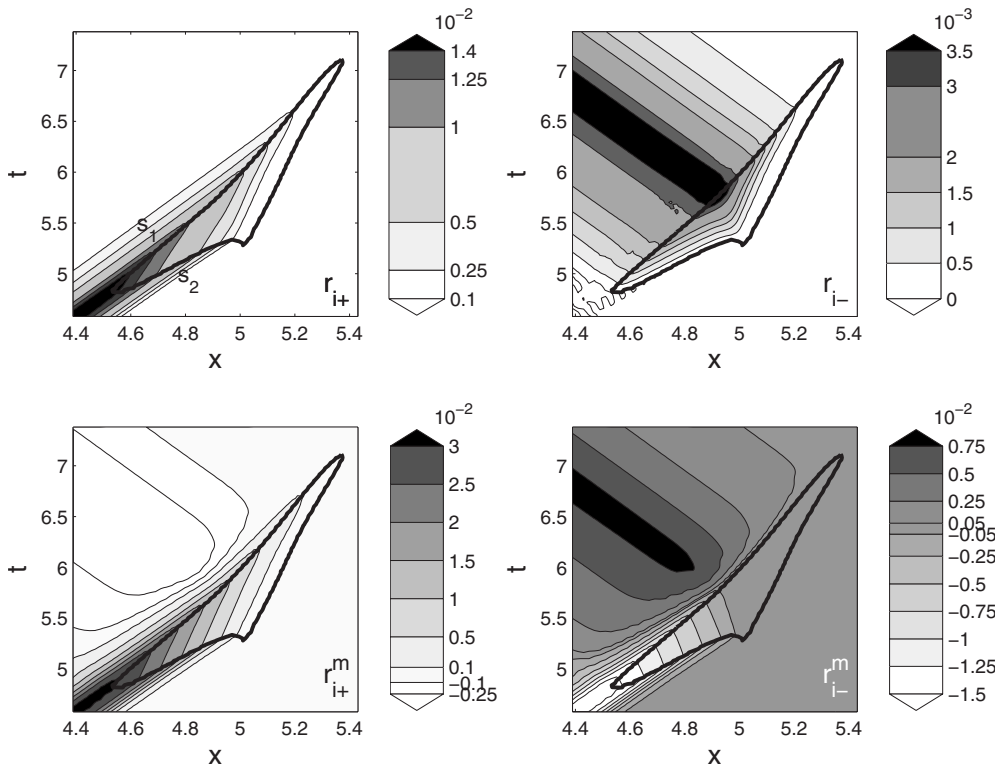


FIG. 10. Hovmöller (characteristic) diagrams of the linearized Riemann variables associated with the dry and moist internal characteristics: $r_{i\pm}$ and $r_{i\pm}^m$, respectively. The precipitating region is delimited by the thick black contour. The lines s_1 and s_2 correspond to a dry internal subsonic front and a moist internal supersonic precipitation front, respectively.

D. Simulation of a warm gravity current over a saturated layer

The second numerical experiment gives an illustration of the capability of the numerical scheme to capture fine details of fully nonlinear fully baroclinic dynamics. As an example,

we consider a “dam-break” problem with a terminating warm dry layer over a saturated cold layer. Physically, this type of flow can represent an upper-level outflow from deep convection.

We initialize the numerical model in such a “dam-break”

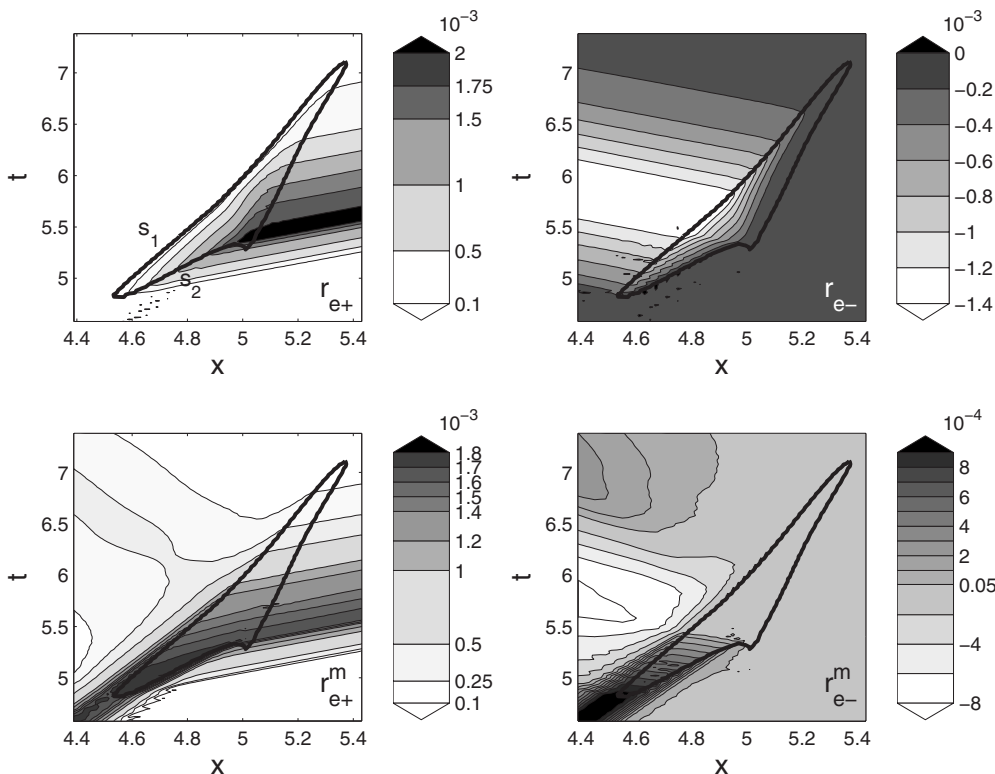


FIG. 11. Hovmöller (characteristic) diagrams of the linearized Riemann variables associated with the dry and moist external characteristics: $r_{e\pm}$ and $r_{e\pm}^m$, respectively. The precipitating region is delimited by the thick black contour. The lines s_1 and s_2 correspond to a dry internal subsonic front and a moist internal supersonic precipitation front, respectively.

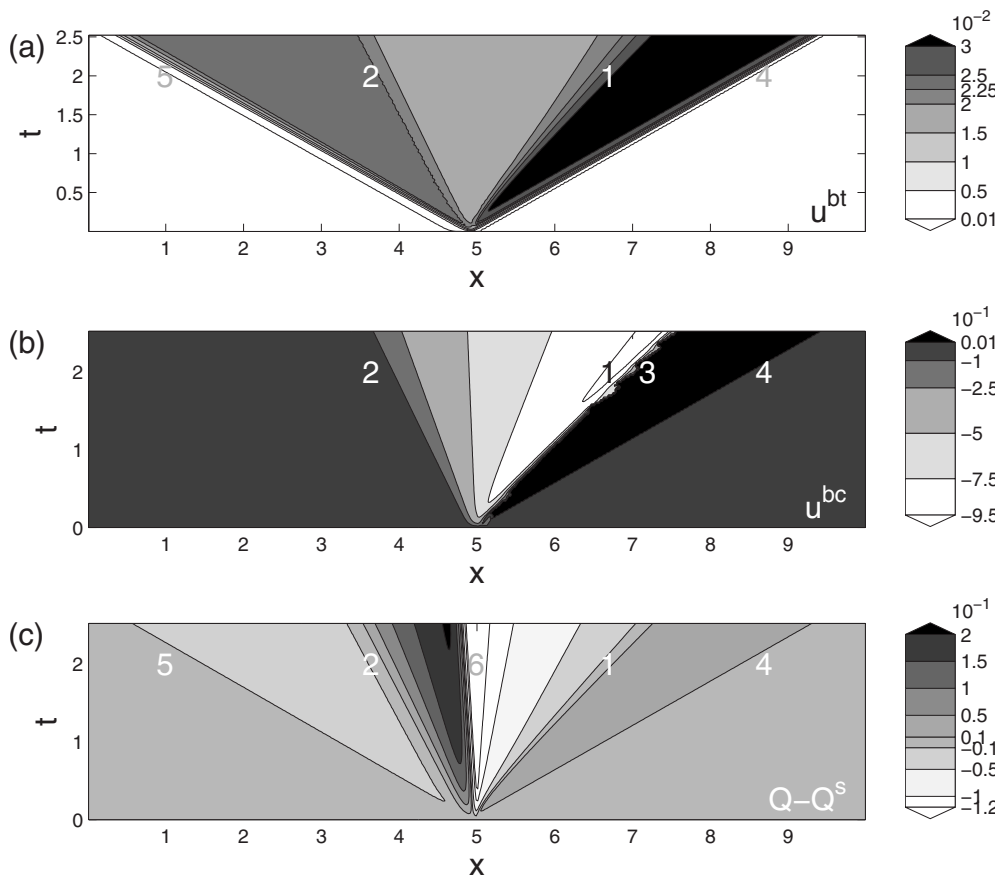


FIG. 12. Hovmöller (characteristic) diagrams of the barotropic u^{bt} (a) and baroclinic u^{bc} (b) velocities and the moisture deficit $Q-Q^s$ (c) for the dry simulation of a dam-break problem. The different fronts are labeled by numbers: 1—warm internal wave ($s_w \approx 0.96$), 2—cold internal wave ($s_c \approx -0.52$), 3—pseudofront arising due to precision drop in u_2 when $h_2 \rightarrow 0$, 4 and 5—weak external gravity waves, and 6—moisture gradient.

problem (which can be related to the genuine dam-break problem, frequently studied with the help of the two-layer shallow-water model, through Table I) with the following interface profile:

$$h_2(x,0) = \begin{cases} H_2 \tanh\{-a(x-x_M)\} & \text{if } x \leq x_M, \\ 0 & \text{if } x \geq x_M, \end{cases} \quad (6.6)$$

where $H_2=1$, $a=10$, and $x_M=5$. The two layers are initially at rest: $u_1(x,0)=u_2(x,0)=0$ and $h_1(x,0)=H_0-h_2(x,0)$, and the lower one is uniformly saturated: $Q(x,0)=Q^s=0.9$. We compare a “dry” simulation for which $P \equiv 0$ at all times and a “moist” one for which precipitation can be triggered.

The initial condition is a nonstationary state and in the absence of rotation, the colder layer will tend to move to the left and the warmer layer to the right, in order to recover the state of static equilibrium. At the initial times, it is expected, cf. Eq. (5.5), that a strong baroclinic velocity appears at the head of the warm current and convergence (divergence) develops at the western (eastern) side of the head. In the full three-dimensional equations, localized convergence (divergence) produces a vertical ascent (descent), cf. Eq. (2.3). Subsequently, such circulation should spread. The calculations confirm this scenario, as shown in the following figures.

Figure 12 presents the Hovmöller (characteristic) diagrams of the barotropic u^{bt} (Fig. 12(a)) and baroclinic u^{bc} (Fig. 12(b)) velocities and the moisture deficit $Q-Q^s$ (Fig. 12(c)) for the dry simulation. We present spatial profiles of the variables at $t=2$ in Fig. 13.

The head front (front 1) corresponds to a warm internal wave and propagates eastward with high velocity: $s_w \approx 0.96$. In fact, the velocity field u_2 quickly grows and the nonlinear advection terms become important. At the warm head, the wave solution rapidly breaks and propagates as a strong shock: $[u_2 h_2] \neq 0$. Its velocity depends on the RH conditions [Eq. (3.45)] completed by the ones selected by our numerical scheme (consistent with layer-wise momentum conservation in each layer²⁸). The front 2 corresponds to a cold internal wave. It propagates more slowly $s_c \approx -0.52$ and follows the internal characteristic ($\sqrt{C_-}=0.56$ for $H_2=1$).

It should be stressed that the would-be front 3 visible in the baroclinic velocity field in Figs. 12(b) and 13 is spurious, as it is not identifiable in the momentum variable $u_2 h_2$. Since the velocity field u_2 is retrieved from the momentum $u_2 h_2$, the precision in u_2 drops for h_2 tending to zero, which explains the noise in the propagation of this pseudofront, which is just a zone of rapid change of u_2 , for $t > 1.5$.

Note that the velocity of these fronts can be derived from the one-layer RSW model,³² assuming that the thickness of the upper layer goes continuously to zero at the head; from the values of the nonlinear Riemann invariants,

$$u(t_0) + 2\sqrt{gh(t_0)} = u(t) + 2\sqrt{gh(t)}, \quad (6.7)$$

one finds, for $u(t_0)=0$ and $h(t_0)=0$ at the head, $s_w=2c(t_0)$ and $s_c=-c(t_0)$, where $c(t_0)=\sqrt{gh(t_0)}$ is the characteristic velocity calculated with respect to the initial state. Our results are in approximate agreement with these latter if we use the linear internal characteristic velocity for $c(t_0)$.

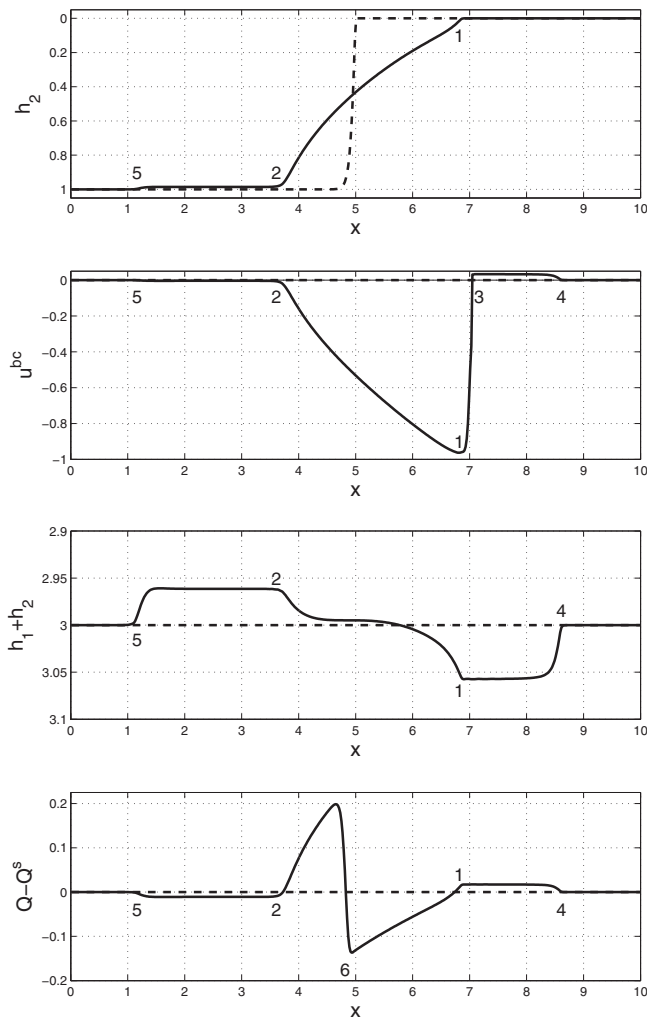


FIG. 13. Spatial profiles of different variables at $t=2$ for the dry simulation of the dam-break problem: the height of the upper layer h_2 , the baroclinic velocity u^{bc} , the total height h_1+h_2 , and the moisture deficit $Q-Q^s$. These profiles are compared to the initial ones denoted by dashed lines. Fronts are labeled by numbers corresponding to Fig. 12.

Since the lower surface is free, a part of the energy is also transferred to external gravity waves (fronts 4 and 5). As clearly seen in the barotropic velocity field (Fig. 12(a)), they propagate faster: $+\sqrt{C_+}=+1.73$ (for $H_2=0$) and $-\sqrt{C_+}=-1.78$ (for $H_2=1$).

The growing anomaly of velocity u_1 induces perturbations in the moisture field. This is shown in Fig. 12(c). A strong moisture gradient (front 6) appears where $\partial_x u_1=0$ and propagates with the velocity $c_q=u_1 \approx -0.06$ following the nonpropagating characteristic. It separates two areas: the ascent area ($\partial_x u_1 < 0$), situated between the cold internal wave (front 2) and the moisture gradient (front 6), which is supersaturated; and the descent area ($\partial_x u_1 > 0$), situated between the moisture gradient (front 6) and the warm internal wave (front 1), which is subsaturated. Note that slightly supersaturated and subsaturated areas also appear due to external wave propagation, between the fronts 1 and 4 and 2 and 5, respectively.

In the moist simulation, a similar scenario is observed in Figs. 14(a)–14(c) but precipitation is now triggered by the ascent motions ($\partial_x u_1 < 0$).

The eastward external gravity wave 4 triggers and maintains precipitation on its way, as expected from Eq. (3.41). The precipitation induces a weak perturbation of h_2 and the front 4 consequently becomes the head front, see the h_2 -profile in Fig. 15.

The cold internal wave (front 2) still propagates following the dry internal characteristic, but it is now followed by a moist subsonic internal precipitation front 7 with a velocity close to the linear moist internal gravity wave speed: $-\sqrt{C_-^m} < s_p \approx -0.4 < 0$ where $\sqrt{C_-^m}=0.41$. A second precipitating region is thus well observed in the ascent area, delimited by this precipitation front 7 and the point where divergence field vanishes $\partial_x u_1=0$ and $Q=Q^s$, the moisture gradient (front 6). Precipitation modifies the Riemann variables and their characteristic velocity in such a way that a plateau appears between 8 and 1 one instead of a monotonic profile. Moreover, the weak disturbances induced by precipitation triggered by the eastward external gravity wave 4 modify the jumps $[u_2]$ and $[h_2]$ of the warm internal wave (front 1) and slow down its propagation: $s_w \approx 0.67$. This is an extension, to a different configuration and to the two-layer model, of the one-layer results presented in Ref. 1.

A complementary experiment would be a lower layer saturated cold gravity current propagating beneath a dry warm upper layer. One can show, however, that precipitation does not occur in this case, with moisture just following the interface.

VII. CONCLUSIONS

We have derived a two-layer RSW model of the precipitating atmosphere. We demonstrated that the model has enjoyable properties conformal to our intuition on moist-convective processes. It reproduces, on one hand, the recently introduced one-layer moist-convective RSW model and, on the other hand, the previously used two-layer quasi-geostrophic model in appropriate limits. While linearized, the model corresponds to the classical baroclinic model.² We studied the properties of the model and described different types of possible discontinuities, including the precipitation fronts. We showed that these latter perfectly correspond to the ones studied recently in the literature in the linearized baroclinic models. We also showed that precipitation moderates the hyperbolicity loss inherent to the two-layer models. The model allows for efficient numerical simulations with the new-generation finite-volume schemes, as we demonstrated in our numerical illustrations. The simulations allowed us to benchmark the numerical scheme and to show that it successfully works in fully nonlinear and fully baroclinic situations; therefore, it can be used for more realistic simulations. Work on the life cycle of the moist baroclinic instability is in progress in the framework of the model.

ACKNOWLEDGMENTS

This work was supported by the French ANR grant SVEMO. GL acknowledges support by foundation MAIF.

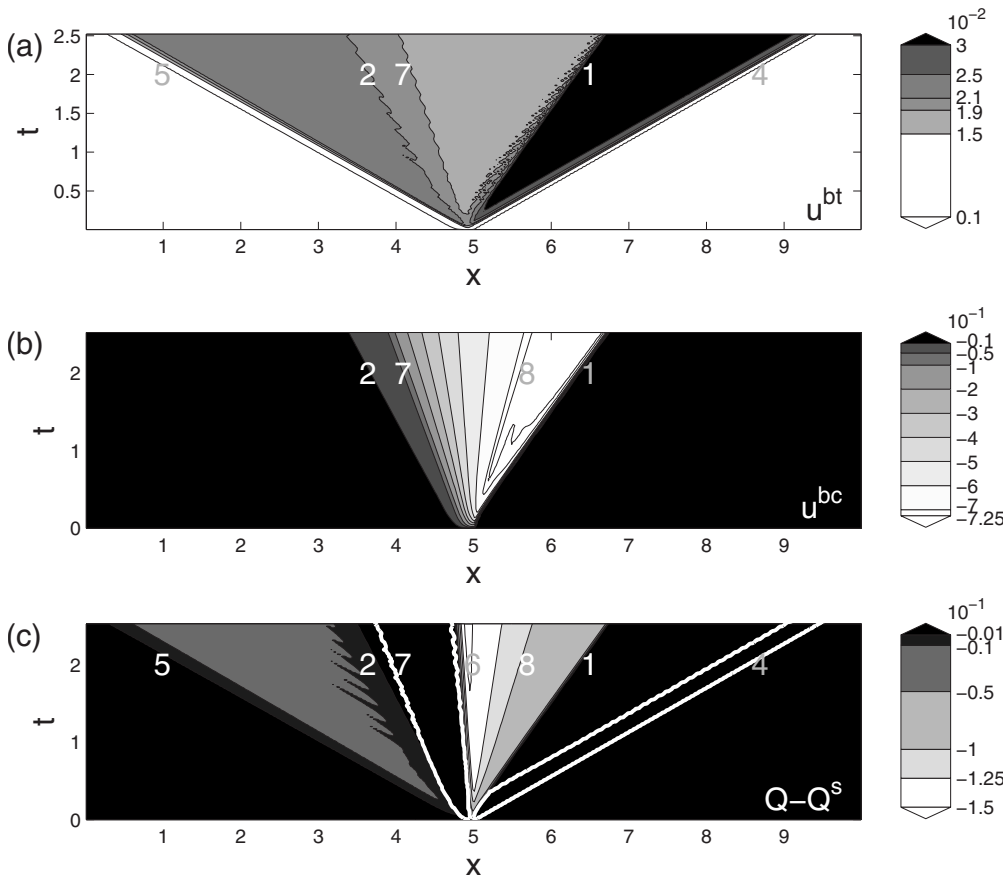


FIG. 14. Same as Fig. 12 but for the moist simulation. The white thick contours delimit the precipitating regions. The first one is localized along the external gravity wave 4 propagation. The second one is bounded from the left by the moist internal subsonic precipitation front 7 ($-\sqrt{C_-^m} < s_p \approx -0.4 < 0$), and from the right by the moisture gradient (front 6). The warm internal wave (front 1) propagates more slowly ($s_w \approx 0.67$) and a plateau appears between fronts 8 and 1.

APPENDIX A: THE TWO-LAYER MOIST-CONVECTIVE RSW MODEL WITH A MASS LOSS (ML-MC2RSW)

1. The model

Another two-layer model can be derived with moisture confined in the lower layer ($Q=Q_1$, $Q_2=0$, and $P_2=0$) but where “convective columns” go through the upper boundary. The additional vertical velocities at the top of each layer are identical and proportional to precipitation in the lower layer: $W_1=W_2=W=\beta P$ ($P=P_1$) with $\theta_2=\theta(z_2)$ and $q(z_2)=0$, see Fig. 16.

This model can be seen as the lower part of a precipitating three-layer model where the mass of the middle-level layer is unaffected. Note that three-layer models (or two-baroclinic-mode models) are considered to be sufficient to model moist convection in the tropics.^{10,33}

In this case, we obtain the following set of equations following the lines of Sec. II:

$$\partial_t \mathbf{v}_1 + (\mathbf{v}_1 \cdot \nabla) \mathbf{v}_1 + f \mathbf{k} \times \mathbf{v}_1 = -g \nabla (h_1 + h_2), \quad (\text{A1})$$

$$\begin{aligned} \partial_t \mathbf{v}_2 + (\mathbf{v}_2 \cdot \nabla) \mathbf{v}_2 + f \mathbf{k} \times \mathbf{v}_2 = & -g \nabla (h_1 + \alpha h_2) \\ & + \frac{\mathbf{v}_1 - \mathbf{v}_2}{h_2} \beta P, \end{aligned} \quad (\text{A2})$$

$$\partial_t h_1 + \nabla \cdot (h_1 \mathbf{v}_1) = -\beta P, \quad (\text{A3})$$

$$\partial_t h_2 + \nabla \cdot (h_2 \mathbf{v}_2) = 0, \quad (\text{A4})$$

$$\partial_t Q + \nabla \cdot (Q \mathbf{v}_1) = -P, \quad (\text{A5})$$

where $\alpha = \theta_2 / \theta_1$ for $\theta_0 = \theta_1$.

2. Conservation laws

From Eq. (3.6), the total energy of the isolated system now always decreases when precipitation occurs ($\beta > 0$),

$$\partial_t E = - \int dx \beta P \left(g(h_1 + h_2) + \frac{(\mathbf{v}_1 - \mathbf{v}_2)^2}{2} + \frac{\mathbf{v}_2^2}{2} \right) \leq 0, \quad (\text{A6})$$

This mainly results from the fact that the total mass $h_1 + h_2$ is not conserved anymore in precipitating regions.

Moist enthalpy in the lower layer, $m_1 = h_1 - \beta Q$, is again locally conserved.

The momentum equations are similar to Eqs. (3.10) and (3.11) except for the upper layer where a new source $-\mathbf{v}_2 \beta P$ appears in the rhs due to the transfer of momentum induced by the moist convection W_2 through the upper boundary. Consequently, the total momentum is no longer locally conserved in the precipitating regions.

The PV Eqs. (3.12) and (3.13) still hold but the first source term in the rhs of the equation for the upper layer disappears since mass h_2 is here locally conserved. In precipitating regions, MPV is a Lagrangian invariant, as in the mc2RSW model, see Eq. (3.14).

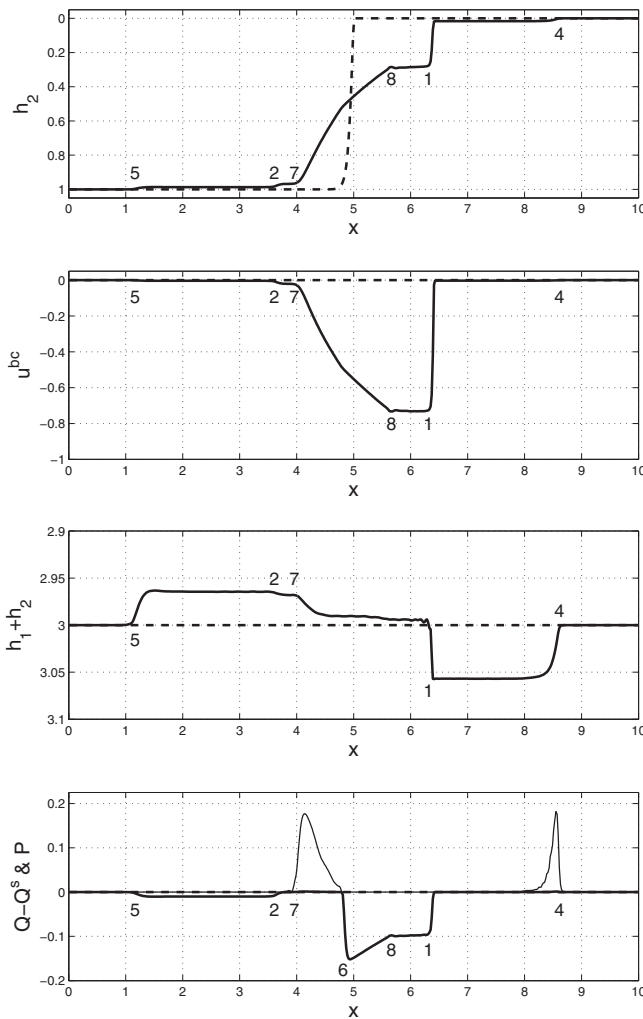


FIG. 15. Same as Fig. 13 but for the moist simulation. Spatial distribution of precipitation at $t=2$ is presented in the lower panel (thin line). The front labeling is the same as in Fig. 14.

3. Mathematical properties

a. Characteristic equation

The characteristic equation is again given by Eq. (3.18) and the linear characteristic velocities [Eq. (3.19)] follow.

In the immediate relaxation limit ($\tau \rightarrow 0$), Eqs. (A2) and

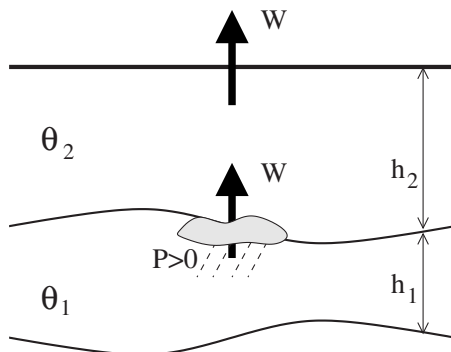


FIG. 16. Sketch of the ml-mc2RSW model.

(A3) can be rewritten, in the precipitating region only, as Eqs. (3.22) and (3.23) with $Q=Q^s$ and $P=Q^s \nabla \cdot \mathbf{v}_1$. The associated characteristic equation in 1.5D is

$$\tilde{\mathcal{F}}^m(c) = \mathcal{F}(c) + \tilde{\mathcal{R}}(c)g\beta Q^s = 0, \tag{A7}$$

where

$$\tilde{\mathcal{R}}(c) = (u_1 - c)(u_1 - u_2) + (u_2 - c)^2 - (\alpha - 1)gh_2, \tag{A8}$$

if nonpropagating characteristics are discarded ($c=u_1$ and $c=u_2$). The moist linear characteristic velocities \tilde{C}_{\pm}^m are given by Eq. (3.19) with

$$\tilde{\Delta}^m = 1 - \frac{4M_1H_2(\alpha - 1)}{(M_1 + \alpha H_2)^2} = \frac{(M_1 - \alpha H_2)^2 + 4M_1H_2}{(M_1 + \alpha H_2)^2}. \tag{A9}$$

Since the argument of the square root is positive for a positive moist enthalpy M_1 , $\tilde{C}_{\pm}^m > 0$ (corresponding c are real) for stable stratification ($\alpha > 1$) and the linearized system [Eqs. (3.21)–(3.24)] is hyperbolic. Contrary to the mc2RSW model, one can show that the inequality between dry and moist linearized characteristic velocities is here the same for the external (+) and the internal (–) modes

$$\tilde{C}_{\pm}^m < C_{\pm}. \tag{A10}$$

The nonlinear moist characteristic velocities [solutions of Eq. (A7)] as functions of the baroclinic velocity u^{bc} are shown in Fig. 17 (dashed black lines). They are compared to solutions of Eq. (3.18) (solid black lines). For $u^{bc}=0$, the inequality [Eq. (A10)] is verified, and for given values of parameters it is maintained until the limiting value $|u^{bc}|/\sqrt{gh_1} \approx 1$. Note that, contrary to the solutions of $\mathcal{R}=0$ in the mc2RSW model, the solutions of $\tilde{\mathcal{R}}(c)=0$ (solid gray line) are not constant and do not allow us to exactly define this limit.

b. Criterion of hyperbolicity

In the nonprecipitating regions, the ml-mc2RSW model does not differ from the mc2RSW model and the sufficient conditions [Eq. (3.35)] still hold. However, in the precipitating regions with the immediate relaxation approximation ($\tau \rightarrow 0$), the moist additional term $\tilde{\mathcal{R}}(c)$ in the characteristic Eq. (A7) depends on the solutions c . Consequently, even if an equation similar to Eq. (3.30) can be derived using appropriate variables (\tilde{p}, \tilde{r}), the relation between them is no more linear and simple geometric considerations do not work.

Figure 18 shows the solutions of Eq. (A7) denoted by dashed black lines in the (p, r) -plane defined by Eq. (3.31). These solutions are asymmetric in r compared to the mc2RSW model, see Fig. 4.

c. Linearized Riemann variables

A linearization can be applied to the 1D version of Eqs. (A1)–(A5), as done in Sec. III C 3,

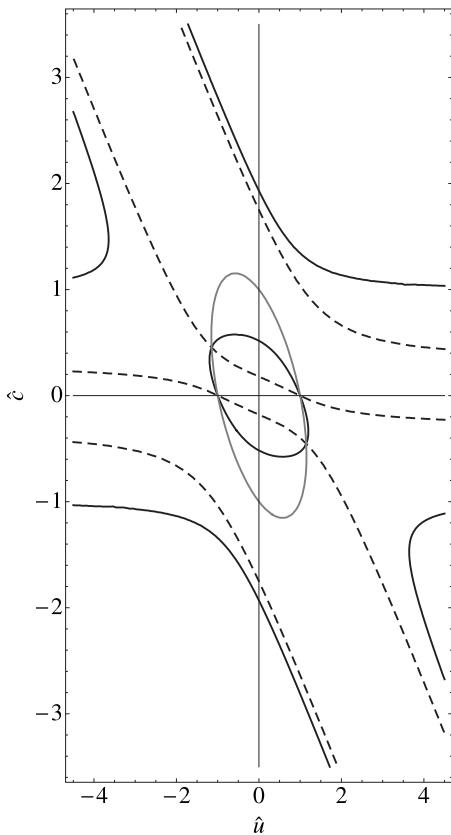


FIG. 17. Same as Fig. 3 for the ml-mc2RSW model. Solid gray line corresponds to solutions of $\tilde{\mathcal{R}}(c)=0$ for which the dry and moist characteristic velocities could be identical, which is the case at the intersections between dry (solid) and moist (dashed) internal (slow) characteristic curves at $|\hat{u}| \approx 1.1$ and $|\hat{c}| \approx 1$.

$$\begin{cases} (\partial_t + c_k \partial_x) r_k = -\frac{c_k}{H_1} \beta P, \\ \partial_t r_0 = -\left(1 - \frac{\beta \bar{Q}}{H_1}\right) P, \end{cases} \quad (\text{A11})$$

where Riemann variables are given by Eq. (3.42). Nothing changes compared to the mc2RSW model, except for the precipitation term in the propagating Riemann variables equations.

In the immediate relaxation limit ($\tau \rightarrow 0$), the Riemann variables in the precipitating regions \tilde{r}_k^m are invariants, as in Eq. (3.43), along the characteristic curves \tilde{c}_k^m , given by positive and negative square roots of \tilde{C}_\pm^m . They are expressed by

$$\tilde{r}_k^m = u_1 + \frac{\tilde{c}_k^m}{M_1} \eta_1 + \left(\frac{\tilde{c}_k^{m2}}{gM_1} - 1\right) \left(u_2 + \frac{\tilde{c}_k^m}{H_2} \eta_2\right). \quad (\text{A12})$$

d. Fronts and Rankine–Hugoniot conditions

Strong shocks.

The results for strong shocks for the 1.5D mc2RSW model [Eq. (3.45)] still hold since precipitation does not appear in the associated RH conditions. Nevertheless, in the special case of a strong shock in a precipitating region only ($P > 0$) and for the immediate relaxation approximation

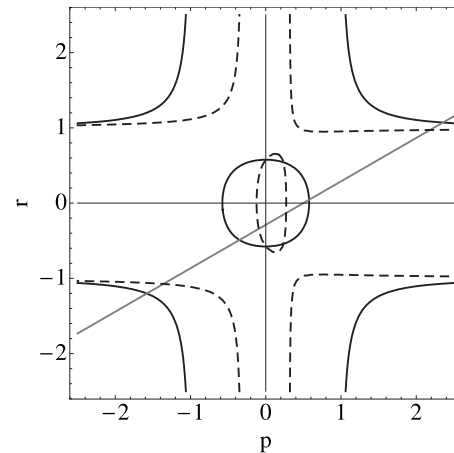


FIG. 18. Same as Fig. 4 for the ml-mc2RSW model.

($\tau \rightarrow 0$), the total momentum equation loses its conservative form due to the term $-\mathbf{v}_2 \beta P$ [see Eq. (A2)] and prevents us from deriving the associated RH conditions.

Precipitation fronts.

The RH conditions for the derivatives of the dynamical variables (supposed to be continuous) are given by Eq. (3.48) with obvious modification of the mass conservation in the upper layer,

$$(u_2 - s)[\partial_x h_2] + h_2[\partial_x u_2] = 0. \quad (\text{A13})$$

Discarding nonpropagating solutions $s = u_1$ and $s = u_2$, two main conditions [Eq. (3.49)] follow, where \mathcal{R} is replaced by $\tilde{\mathcal{R}}(c)$ given by Eq. (A8). The linearization of the coefficients in front of jumps in these equations around a state of rest gives expressions identical to Eq. (3.50), where C_\pm^m is replaced by \tilde{C}_\pm^m . In the configuration $P_- = 0$ ($[\partial_x Q] < 0$ and $[P] > 0$), five types of precipitation fronts are found for $\alpha > 1$. Since $\tilde{C}_+^m < C_+ < C_+^m$, these fronts correspond to the ones found for the mc2RSW model for which C_+ , C_+^m , and C_-^m are replaced by \tilde{C}_+^m , C_+ , and \tilde{C}_-^m , respectively.

Nonlinear precipitation front velocities s are shown in Figs. 19 and 20 as functions of the baroclinic velocity u^{bc} for the configuration $P_- = 0$. As in the mc2RSW model, linearized results are well verified for $u^{bc} = 0$: precipitation fronts 1 to 4 are presented in Fig. 19 and the fifth in Fig. 20.

4. Comparison with the mc2RSW model

As the mc2RSW model, the ml-mc2RSW model gives dry and moist internal characteristic velocities in agreement with observations.¹⁶ The properties of the precipitation fronts are the same. However, the main advantage of the mc2RSW model is its total mass conservation. Moreover, the total energy in the mc2RSW model increases in precipitating regions in the first approximation, conformal to the idea of the latent heat release by condensation, while it always decreases in the ml-mc2RSW model due to the mass loss. Finally, a criterion of hyperbolicity can be easily derived in the mc2RSW model, which is not the case for the ml-mc2RSW one.

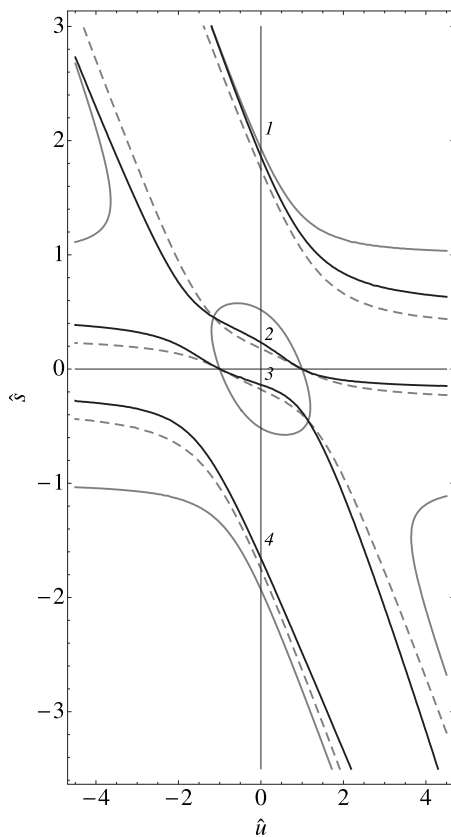


FIG. 19. Same as Fig. 5 for ml-mc2RSW model.

APPENDIX B: DEPENDENCE OF THE SATURATION THRESHOLD ON THE LOWER LAYER THICKNESS

As shown in Appendix B of Ref. 1, the saturation threshold Q^s can depend on the moist lower layer thickness $h_1 = H_1 + \eta_1$. In the first approximation, one can assume the linear expression $Q^s = Q_0^s - \nu \eta_1$ where Q_0^s and ν are constant and the last term corresponds to a linearization of the Clausius–Clapeyron equation. In this case, all the results presented in the main body of the paper still hold with the replacement of Q^s by

$$Q_{eff}^s = \frac{Q_0^s + \nu H_1}{1 + \nu \beta}, \quad (\text{B1})$$

in the equations corresponding to precipitating regions in the immediate relaxation limit ($\tau \rightarrow 0$) as in Ref. 6, and thus in the expressions for the moist characteristic velocities.

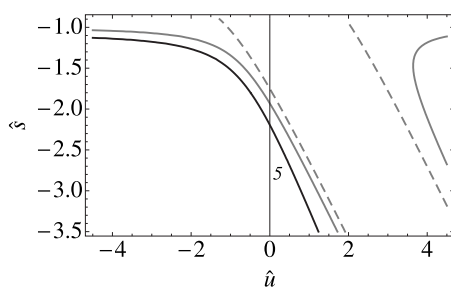


FIG. 20. Same as Fig. 6 for ml-mc2RSW model.

- ¹F. Bouchut, J. Lambaerts, G. Lapeyre, and V. Zeitlin, “Fronts and nonlinear waves in a simplified shallow-water model of the atmosphere with moisture and convection,” *Phys. Fluids* **21**, 116604 (2009).
- ²A. E. Gill, “Studies of moisture effects in simple atmospheric models: The stable case,” *Geophys. Astrophys. Fluid Dyn.* **19**, 119 (1982).
- ³D. M. W. Frierson, A. J. Majda, and O. M. Pauluis, “Large scale dynamics of precipitation fronts in the tropical atmosphere: A novel relaxation limit,” *Commun. Math. Sci.* **2**, 591 (2004).
- ⁴S. N. Stechmann and A. J. Majda, “The structure of precipitation fronts for finite relaxation time,” *Theor. Comput. Fluid Dyn.* **20**, 377 (2006).
- ⁵O. Pauluis, D. M. W. Frierson, and A. J. Majda, “Precipitation fronts and the reflection and transmission of tropical disturbances,” *Q. J. R. Meteorol. Soc.* **134**, 913 (2008).
- ⁶G. Lapeyre and I. M. Held, “The role of moisture in the dynamics and energetics of turbulent baroclinic eddies,” *J. Atmos. Sci.* **61**, 1693 (2004).
- ⁷B. J. Hoskins and F. P. Bretherton, “Atmospheric frontogenesis models: Mathematical formulation and solution,” *J. Atmos. Sci.* **29**, 11 (1972).
- ⁸K. A. Emanuel, *Atmospheric Convection* (Oxford University, New York, 1994), Chap. 4.
- ⁹V. Zeitlin, “Introduction: Fundamentals of rotating shallow water model in the geo-physical fluid dynamics perspective,” *Nonlinear Dynamics of Rotating Shallow Water: Methods and Advances*, edited by V. Zeitlin (Elsevier, Amsterdam, 2007), Chap. 1.
- ¹⁰D. A. Schecter and T. J. Dunkerton, “Hurricane formation in diabatic Ekman turbulence,” *Q. J. R. Meteorol. Soc.* **135**, 823 (2009).
- ¹¹A. K. Betts and M. J. Miller, “A new convective adjustment scheme. Part II: Single columns tests using GATE wave, BOMEX, ATEX and arctic air-mass data sets,” *Q. J. R. Meteorol. Soc.* **112**, 693 (1986).
- ¹²J. R. Holton, *An Introduction to Dynamic Meteorology* (Academic, London, 1972).
- ¹³J. Lambaerts, G. Lapeyre, and V. Zeitlin, “Moist vs dry barotropic instability in a shallow water model of the atmosphere with moist convection,” *J. Atmos. Sci.* **68** (2011).
- ¹⁴G. B. Whitham, *Linear and Nonlinear Waves* (Wiley, New York, 1974), Chap. 5.
- ¹⁵M. J. Castro, P. G. LeFloch, M. L. Munoz-Ruiz, and C. Parés, “Why many theories of shock waves are necessary: Convergence error in formally path-consistent schemes,” *J. Comput. Phys.* **227**, 8107 (2008).
- ¹⁶M. Wheeler and G. N. Kiladis, “Convectively coupled equatorial waves: Analysis of clouds and temperature in the wavenumber-frequency domain,” *J. Atmos. Sci.* **56**, 374 (1999).
- ¹⁷L. V. Ovsyannikov, “Two-layer “shallow water” model,” *J. Appl. Mech. Tech. Phys.* **20**, 127 (1979).
- ¹⁸P. D. Lax, “Hyperbolic systems of conservation laws and the mathematical theory of shock waves,” *SIAM Regional Conference Series in Applied Math*, 1973.
- ¹⁹P. J. Montgomery and T. B. Moodie, “Analytical and numerical results for flow and shock formation in two-layer gravity currents,” *J. Aust. Math. Soc. Ser. B, Appl. Math.* **40**, 35 (1998).
- ²⁰C. S. Yih and C. R. Guha, “Hydraulic jump in a fluid system of two-layers,” *Tellus* **7**, 358 (1955).
- ²¹J. B. Klemp, R. Rotunno, and W. C. Skamarock, “On the propagation of internal bores,” *J. Fluid Mech.* **331**, 81 (1997).
- ²²D. M. Holland, D. S. R. Rosales, and E. G. Tabak, “Internal hydraulic jumps and mixing in two-layer flows,” *J. Fluid Mech.* **470**, 63 (2002).
- ²³Q. Jiang and R. B. Smith, “Ideal shocks in 2-layer flow,” *Tellus* **53A**, 129 (2001).
- ²⁴J. L. Sommer, S. B. Medvedev, R. Plougonven, and V. Zeitlin, “Singularity formation during relaxation of jets and fronts toward the state of geostrophic equilibrium,” *Commun. Nonlinear Sci. Numer. Simul.* **8**, 415 (2003).
- ²⁵V. Zeitlin, G. M. Reznik, and M. B. Jelloul, “Nonlinear theory of geostrophic adjustment. Part 2. Two-layer and continuously stratified primitive equations,” *J. Fluid Mech.* **491**, 207 (2003).
- ²⁶J. Pedlosky, *Geophysical Fluid Dynamics* (Springer-Verlag, New York, 1979).
- ²⁷G. K. Vallis, *Atmospheric and Oceanic Fluid Dynamics* (Cambridge University, Cambridge, 2006).
- ²⁸F. Bouchut and V. Zeitlin, “A robust well-balanced scheme for multi-layer shallow water equations,” *Discrete Contin. Dyn. Syst., Ser. B* **13**, 4 (2010).
- ²⁹J. Gula and V. Zeitlin, “Instabilities of buoyancy-driven coastal currents and their nonlinear evolution in the two-layer rotating shallow-water model. Part 1. Passive lower layer,” *J. Fluid Mech.* **659**, 69 (2010).

- ³⁰M. J. Castro, J. Macías, and C. Parés, “A Q-scheme for a class of systems of coupled conservation laws with source term. Application to a two-layer 1-D shallow water system,” *Math. Modell. Numer. Anal.* **35**, 107 (2001).
- ³¹F. Bouchut, “Efficient numerical finite volume schemes for shallow water models,” in *Nonlinear Dynamics of Rotating Shallow Water: Methods and Advances*, edited by V. Zeitlin (Elsevier, Amsterdam, 2007), Chap. 4.
- ³²G. H. Keulegan, “Wave motion,” in *Engineer Hydraulics*, edited by H. Rouse (Wiley, New York, 1950), pp. 711–768.
- ³³S. N. Stechmann and A. J. Majda, “Gravity waves in shear and implications for organized convection,” *J. Atmos. Sci.* **66**, 2579 (2009).